

1 **Geologic and geomorphic controls on rockfall hazard: how well do past rockfalls predict**  
2 **future distributions?**

3  
4 Josh Borella <sup>1,2</sup>, Mark Quigley <sup>3,2</sup>, Zoe Krauss <sup>4,1</sup>, Krystina Lincoln <sup>5,1</sup>, Januka Attanayake <sup>3</sup>,  
5 Laura Stamp <sup>5,1</sup>, Henry Lanman <sup>6,1</sup>, Stephanie Levine <sup>7,1</sup>, Sam Hampton <sup>1,2</sup>, Darren Gravley <sup>1,2</sup>  
6

7 <sup>1</sup> Frontiers Abroad, 3 Harbour View Terrace, Christchurch, 8082, New Zealand

8 <sup>2</sup> Department of Geological Sciences, University of Canterbury, Christchurch, 8041, New Zealand

9 <sup>3</sup> School of Earth Sciences, The University of Melbourne, Victoria, 3010, Australia

10 <sup>4</sup> Department of Geology, Colorado College, Colorado Springs, CO, 80903, USA

11 <sup>5</sup> Department of Geosciences, Williams College, Williamstown, MA, 01267, USA

12 <sup>6</sup> Department of Geology, Whitman College, Walla Walla, WA, 99362, USA

13 <sup>7</sup> Department of Geology, Carleton College, Northfield, MN, 55057, USA  
14

15 Correspondence: Josh Borella (josh@frontiersabroad.com)  
16

17 *KEYWORDS: Rockfall hazard, boulder spatial distributions, frequency-volume distributions,*  
18 *Canterbury Earthquake Sequence, prehistoric rockfall boulders, deforestation, rockfall*  
19 *source characteristics, rockfall physical properties, rockfall numerical modelling,*  
20 *Christchurch*  
21

22 **Abstract**  
23

24 To evaluate the geospatial hazard relationships between recent (contemporary) rockfalls and  
25 their prehistoric predecessors, we compare the locations, physical characteristics, and  
26 lithologies of rockfall boulders deposited during the 2010-2011 Canterbury earthquake  
27 sequence (CES) (n=185) with those deposited prior to the CES (n=1093). Population ratios of  
28 pre-CES to CES boulders at two study sites vary spatially from ~5:1 to 8.5:1. This is interpreted  
29 to reflect (i) variations in CES rockfall flux due to intra- and inter-event spatial differences in  
30 ground motions (e.g. directionality) and associated variations in source cliff responses, (ii)  
31 possible variations in the triggering mechanism(s), frequency, flux, record duration, boulder  
32 size distributions, and post-depositional mobilization of pre-CES rockfalls relative to CES  
33 rockfalls, and (iii) geological variations in the source cliffs of CES and pre-CES rockfalls. On  
34 interfluvial, CES boulders traveled approximately 100 to 250 m further downslope than  
35 prehistoric (pre-CES) boulders, interpreted to reflect reduced resistance to CES rockfall  
36 transport due to preceding anthropogenic hillslope de-vegetation. Volcanic breccia boulders  
37 are more dimensionally equant, rounded, larger, and traveled further downslope than coherent  
38 lava boulders, illustrating clear geological control on rockfall hazard. In valley bottoms, the  
39 furthest-traveled pre-CES boulders are situated further downslope than CES boulders due to  
40 (i) remobilization of pre-CES boulders by post-depositional processes such as debris flows,  
41 and (ii) reduction of CES boulder velocities and travel distances by collisional impacts with  
42 pre-CES boulders. A considered earth-systems approach is required when using preserved  
43 distributions of rockfall deposits to predict the severity and extents of future rockfall events.

## 44 **1 Introduction**

45

46 Rockfall deposits pervade many mountainous and hilly regions worldwide (Varnes, 1978;  
47 Evans and Hungr, 1993; Wieczorek, 2002; Dorren, 2003; Guzzetti et al., 2003) and can provide  
48 important data for assessing future rockfall hazards (Porter and Orombelli, 1981; Keefer, 1984;  
49 Dussauge-Peisser et al., 2002; Copons and Vilaplana, 2008; Wieczorek et al., 2008; Stock et  
50 al., 2014; Borella et al., 2016a). Their characteristics (e.g. location, size, morphology) may be  
51 used to complement numerical rockfall modeling scenarios (Agliardi and Crosta, 2003; Dorren  
52 et al., 2004; Heron et al., 2014; Vick, 2015; Borella et al., 2016a) and inform engineering-  
53 design criteria for rockfall mitigation structures (e.g. impact fences, tiebacks, protection  
54 forests) (e.g. Agliardi and Crosta, 2003; Dorren et al., 2004; Guzzetti et al., 2004). However,  
55 natural and anthropogenic changes to the landscape (including changes to the rockfall source  
56 and slope areas) between successive rockfall events and the post-depositional history for  
57 rockfalls can be complex (e.g. Borella et al., 2016a,b). To better understand how past rockfalls  
58 provide suitable proxies for characterizing future hazard, comparisons between the geologic  
59 and geomorphic attributes of individual rockfall events and cumulative amalgamations of many  
60 events are valued. Critical evaluations of possible intervening changes to the landscape that  
61 may influence the mechanics of rockfall production and travel are an important component of  
62 these studies.

63

64 More than 7000 mapped individual rocks fell from cliffs in the Port Hills in southern  
65 Christchurch during the 2010-2011 Canterbury Earthquake Sequence (CES) in New Zealand's  
66 South Island (Massey et al., 2014). Most of the rockfalls (>6000) occurred during the 22  
67 February 2011 moment magnitude (Mw) 6.2 and 13 June 2011 Mw 6.0 Christchurch  
68 earthquakes (Massey et al., 2014). Approximately 200 houses were impacted, 100 houses  
69 severely damaged, and five fatalities caused by falling rocks in the 2011 February earthquake  
70 (Massey et al., 2014; Grant et al., 2018). CES rockfalls were characterized by boulder-size  
71 distribution, runout distance (the distance a rock travels down a slope from its source), source-  
72 area dimensions, and boulder-production rates over a range of triggering peak ground  
73 accelerations (Massey et al., 2012a-e, 2014, 2017; Quigley and Mackey, 2014; Quigley et al.,  
74 2016).

75

76 Subsequent field investigations revealed an abundance of pre-CES rockfall deposits in CES  
77 rockfall areas (Townsend and Rosser, 2012; Mackey and Quigley, 2014; Borella et al.,

78 2016a,b), suggesting multiple rockfall events had occurred at these sites in the past (Mackey  
79 and Quigley, 2014; Borella et al., 2016a,b; Sohbati et al., 2016). Retrospectively, these pre-  
80 CES deposits had potential value to contribute to hazard assessments during land-planning and  
81 urban development in Christchurch prior to the CES; however, there is no evidence that they  
82 did so (Townsend and Rosser, 2012; Litchfield et al., 2016). At one well-studied location  
83 (Rapaki) in the Port Hills of southern Christchurch, CES and pre-CES boulder populations  
84 were shown to have similar volumetric size and morphology characteristics, but a significant  
85 population of CES boulders had longer maximum runout distances than their pre-CES  
86 counterparts (Borella et al., 2016a). Pre-CES rockfalls were dated using independent  
87 approaches to >3-15 ka (Mackey and Quigley, 2014; Sohbati et al., 2016; Borella et al., 2016b).  
88 With the aid of numerical modeling of rockfall trajectories (using RAMMS - rapid mass  
89 movement simulation) these data were collectively interpreted to suggest that anthropogenic  
90 deforestation between pre-CES and CES rockfalls was the primary cause for the observed  
91 spatial distinctions in CES and pre-CES rockfall distributions (Borella et al., 2016a). Elsewhere  
92 in the Port Hills and greater Banks Peninsula, the causes for differences in the spatial  
93 distribution between CES and pre-CES rockfalls are less clear and in some locations the current  
94 positions of pre-CES boulders extend further distances from source cliffs than their CES  
95 counterparts. **A more integrated and regional understanding of the geologic, geomorphic,  
96 seismogenic, and anthropogenic controls on rockfall distributions has the potential to inform  
97 rockfall hazard analyses for land-zoning and engineering considerations here and elsewhere  
98 (e.g. Lan et al., 2010).**

99

100 In this study we document the location, volume, morphology, and lithology for individual  
101 (n=1093) pre-CES rockfall boulders at two sites (Rapaki and Purau) in the Banks Peninsula  
102 near Christchurch, New Zealand. The spatial distributions and physical attributes for pre-CES  
103 boulders are compared to rockfall boulders (n=185) deposited at the same sites during the 2010-  
104 2011 CES. RAMMS bare-earth and forested numerical modelling scenarios are conducted to  
105 help evaluate the influence of **natural and** anthropogenic factors on rockfall distributions,  
106 identify boulder sub-populations that have likely experienced post-placement mobility,  
107 determine the relative timing of pre-existing rockfalls (i.e. prehistoric or historic), and evaluate  
108 the efficacy of RAMMS in replicating empirical CES and prehistoric boulder spatial  
109 distributions. We highlight the complexity of interpreting future rockfall hazard based on  
110 former boulder distributions (particularly location) due to: (i) potential landscape changes  
111 including deforestation, (ii) changes in rockfall source (e.g. progressive emergence of bedrock

112 sources from beneath sedimentary cover), (iii) remobilization of prior rockfalls by surface  
113 processes including debris flows (primarily in channels), (iv) lithological variability effects on  
114 the type of material liberated in successive events, (v) collisional impedance with pre-existing  
115 boulders (particularly in channels/valleys), and (vi) variations in the location, size, and strong  
116 ground motion characteristics of past rockfall-triggering earthquakes and their impact on  
117 rockfall flux and boulder mobility. We use an integrated earth-systems approach, which  
118 combines a consideration of geologic, geomorphic, seismogenic, and anthropogenic influences  
119 on rockfall distributions with high-quality field-based (i.e. prehistoric and contemporary  
120 rockfall data sets) and instrumentally-recorded (seismic) data sets, and numerical modeling.  
121 Our results have broad implications for using rockfall distributions to forecast future rockfall  
122 hazard.

123

124

## 125 **2 Geologic Setting**

126

### 127 **2.1 Overview**

128

129 Banks Peninsula, located on the east coast of New Zealand's South Island, is comprised of  
130 three main volcanoes (Lyttelton, Akaroa, and Mt. Herbert) active between 11.0 and 5.8 Ma  
131 (Hampton and Cole, 2009) (Fig. 1). The two study sites (Rapaki and Purau) are located within  
132 the inner crater rim of the Lyttelton Volcanic complex (Figs. 1, 2, 3), the oldest of the volcanic  
133 centers and thought to be active from 11.0 to 9.7 Ma (Hampton and Cole, 2009). Source rock  
134 at both sites is classified by Sewell (1988) and Sewell et al. (1992) as part of the Lyttelton  
135 Volcanic Group (LVG) and consists of basaltic to trachytic lava flows interbedded with breccia  
136 and tuff (Mvl). Numerous dikes and minor domes are observed within the LVG. Our field  
137 observations support the reported lithologic descriptions for the two study locales. The inferred  
138 strike and dip for lava flows nearest to the study sites indicates a shallow inclination in a  
139 predominantly northerly direction for measurements nearest the Rapaki and Purau study sites  
140 (Hampton and Cole, 2009). Sewell et al. (1992) reports a similar shallow northerly to  
141 northwesterly dip of 12° for lava flows nearest Rapaki. The study areas were selected because  
142 both have abundant pre-CES and CES rockfall boulders (Fig. 4) derived from lithologically  
143 equivalent volcanic source rocks. Rapaki represents a case study location proximal to the  
144 source of the 2011 February and June Christchurch earthquakes (epicenters ~2.5-5.0 km;  
145 hypocenters ~ 5.6-7.0 km), while Purau is located more distally (epicenters ~6.6-8.4 km;

146 hypocenters ~8.9-10.3 km). Estimated rockfall-generating peak horizontal ground velocities  
147 (PGV) at the Rapaki site in the February and June earthquakes were  $\geq 30 \text{ cm s}^{-2}$  (Mackey and  
148 Quigley, 2014).

149

## 150 **2.2 Rapaki study site**

151

152 The Rapaki study site is situated in the Port Hills of southern Christchurch (Figs. 1, 2) on the  
153 southeastern slope of Mount Rapaki (*Te Poho o Tamatea*), which has a summit height of ~400  
154 meters. The study hillslope is slightly concave to planar with a total area of ~0.21 km<sup>2</sup> and  
155 faces to the east-southeast. The source zone consists of steep to subvertical bedrock cliffs  
156 composed of stratified basaltic lava and indurated auto-breccia or pyroclastic flow deposits  
157 (Fig. 5A-C). Breccia layers are thicker (~3-10 meters) and jointing is more widely spaced  
158 (often >10 m). Coherent lava layers are comparably thin (<3 meters) and joints are more closely  
159 spaced (generally <1-2 meter). Total height and length of the source rock are ~60 meters and  
160 ~300 meters, respectively (Fig. 5A). Below the source area, is a ~23°, grassy hillslope  
161 composed of windblown sediment deposits (loess), loess and volcanic colluvium, and  
162 overlying rockfall boulders (both CES and pre-CES) (Bell and Trangmar, 1987). Rapaki village  
163 (estimated population=100 residents) lies at the hillslope base at elevations of ~70 meters (asl)  
164 to sea level (Figs. 3, 4). Anthropogenic deforestation has exposed a hillslope that is currently  
165 experiencing accelerated erosion (Borella et al., 2016a,b) in the form of mass wasting and  
166 tunnel gully formation. Shallow landslides, including debris and earth flows, are most prevalent  
167 in upper to mid-slope positions, while rill and gully erosion predominate in lower slope  
168 positions. Rockfall is a dominant surface feature at the Rapaki study site (Mackey and Quigley,  
169 2014; Vick, 2015; Borella et al., 2016a,b). Pre-CES and CES rockfall boulders at the study site  
170 are divided into two dominant lithology types: volcanic breccia (VB) and coherent lava (CL)  
171 basalt. During the 22 February and 13 June 2011 earthquakes, more than 650 individual CES  
172 boulders ranging in diameter from <15 cm to >3m were dislodged from the volcanic source  
173 rock near the top of Mount Rapaki, many impacting and destroying residential homes (Massey  
174 et al., 2014; Mackey and Quigley, 2014).

175

## 176 **2.3 Purau study site**

177

178 Purau is located on the southern side of Lyttelton Harbour, approximately 5 kilometers  
179 southeast of Rapaki (Figs. 1, 3). Slopes at Purau have a west-northwest aspect, the opposite of

180 the Rapaki study hillslope. Mapping of pre-CES and CES rockfall was performed on and within  
181 several interfluves (spurs) and bounding valleys, respectively (Fig. 3) and encompassed a total  
182 area of  $\sim 1.4$  km<sup>2</sup>. The source rock geology at Purau, including lithology and structure, is  
183 equivalent to that observed at Rapaki (Fig. 5D,E). The ridgeline (i.e. volcanic source rock) to  
184 the east obtains a maximum elevation of  $\sim 440$  meters. Locally, individual vertical to subvertical  
185 bluff faces are estimated to be  $\sim 20$ - $30$  meters in height. From the base of the volcanic source  
186 rock, slopes extend downward toward Purau Bay at angles ranging from  $\sim 30^\circ$  to  $\sim 5^\circ$  near Camp  
187 Bay Road (Fig. 3). Field observations indicate the volcanic rock is overlain by loess, loess- and  
188 volcanic-colluvium, and pre-CES and CES rockfall boulders of small (e.g.  $< 1$  m<sup>3</sup>) to extremely  
189 large size (e.g.  $> 100$  m<sup>3</sup>). Deforestation of Purau slopes has left the hillside covered primarily  
190 in low-lying grass and bush. Shallow slips are abundant and are commonly observed on steep  
191 slopes, including valley flanks. Maximum landslide depth is typically  $\sim 1$ - $1.5$  meters and often  
192 exposes volcanic bedrock at bottom, indicating the overlying sediment is relatively thin. Tunnel  
193 gully erosion predominates on canyon flanks and at lower elevations.

194

### 195 **3 Methods**

196

#### 197 **3.1 Field mapping and characterization of CES and pre-CES rockfall boulders**

198

199 We mapped 1276 individual rockfall boulders at the Rapaki (pre-CES=408; CES=48) and  
200 Purau (pre-CES=684; CES=136) study sites for boulder volume  $\geq 1.0$  m<sup>3</sup> (see Supplementary  
201 Data, Tables S1-S4, doi:10.5061/dryad.9km1t86). Where safety conditions permitted, pre-CES  
202 and CES rockfall boulders were mapped to the base of the volcanic source rock. Location  
203 (latitude/longitude) and elevation (meters above sea level) were recorded for each rockfall  
204 deposit using a hand-held Garmin GPSMap 62s device. Boulder dimensions (i.e. height, length,  
205 width) were tape measured in the field. For pre-CES boulders partially buried to the degree  
206 that only two dimensions were adequately measurable, the shorter of the two measured lengths  
207 was used for the 3<sup>rd</sup> dimension, thus insuring a conservative boulder size estimate. No rounding  
208 factor was applied to volumetric estimations of pre-CES boulders. The lithology type was  
209 determined for each pre-CES boulder and was based primarily upon the observed dominant  
210 rock 'texture'. Boulder lithologies were categorized as VB or CL. Transitional lithologies were  
211 rarely observed ( $< 1\%$  of total) and assigned as VB or CL based on the volumetrically  
212 predominant rock type.

213

### 214 **3.2 Boulder runout distance**

215

216 Boulder runout distance was determined by measuring the shortest horizontal and ground-  
217 length distances, perpendicular to slope contour lines, from the nearest potential bedrock source  
218 areas to mapped boulder locations using Google Earth Professional (see Supplementary Data,  
219 Tables S5-S8, doi:10.5061/dryad.9km1t86). Runout distance was calculated for 409 pre-CES  
220 boulders and 48 CES boulders (for volume  $\geq 1.0 \text{ m}^3$ ) at Rapaki. Due to safety concerns we  
221 were unable to record locations for pre-CES boulders within  $\sim 100$  meters (map-length) of the  
222 volcanic source rock at this site. However, boulder frequency counts (for boulder volume  $\geq 0.1$   
223  $\text{m}^3$ ) were field measured within a  $300 \text{ m}^2$  area at distances of 0-10 meters ( $n=31$ ), 30-40 meters  
224 ( $n=35$ ), 60-70 meters ( $n=77$ ), and 100-110 ( $n=24$ ) meters from the volcanic source rock (see  
225 Appendix 1, Fig. A1). The boulder frequency counts at these distances were used to extrapolate  
226 the number of boulders across remaining sections of the study site, consistent with visual  
227 inspection of air photos. At Purau, four separate geomorphic domains (PD1-PD4) were created  
228 to evaluate pre-CES and CES boulder runout distance (see Fig. 3; Supplementary Tables S7,  
229 S8, doi:10.5061/dryad.9km1t86). The domains include interfluvial and valley morphologies and  
230 target areas with both CES and pre-CES rockfall boulders, and cases where the pre-CES  
231 rockfalls were sourced from a single or limited number of rock exposures. We generally report  
232 map-length runout distance within this paper.

233

234 We used the empirical shadow angle method (Lied, 1977; Evans and Hungr, 1993) to analyze  
235 the travel distance of rockfalls at Rapaki and Purau. The shadow angle is the arctangent of the  
236 relationship  $Ht/Lt$ , where  $Ht$  is the height of fall on the talus slope (elevation difference between  
237 the apex of the talus slope and final emplacement location of the rockfall block) and  $Lt$  is the  
238 travel distance on the talus slope (horizontal distance between the apex of the talus slope and  
239 the final emplacement location of the rockfall block) (see Copons, 2009; Lied, 1977; Evans  
240 and Hungr, 1993) (see Appendix 1, Fig. A2). The shadow angle method is most suitable for  
241 our study (compared to the reach or 'Fahrboschung' angle) because it does not require  
242 identifying the source release location for individual rockfall blocks, a parameter we are unable  
243 to determine for the pre-CES and CES rockfalls.

244

### 245 **3.3 RAMMS rockfall modeling**

246

247 Three model scenarios were conducted using the Rapid Mass Movements System (RAMMS)  
248 software (Bartelt et al., 2013; Leine et al., 2014). RAMMS\_1 represents a bare-earth CES  
249 model and was performed to test the reliability of RAMMS in replicating the spatial  
250 distribution for CES rockfalls at Purau. RAMMS\_2 assumes a vegetated slope and simulates  
251 hillslope conditions prior to deforestation (i.e. prehistoric). RAMMS\_3 models the potential  
252 future rockfall hazard at Purau and assumes a bare-earth (deforested) hillslope and dry soil  
253 moisture conditions to insure a worst-case (conservative) outcome. Please see Supp.  
254 Information for more detail on the individual RAMMS modeling scenarios.

255

256 The Purau terrain was modelled using a 4-m DEM (digital elevation model) derived from  
257 LIDAR (light detection and ranging) surveys to model CES (bare-earth scenario) and pre-CES  
258 (prehistoric forested slope scenario) rockfall distributions. The rockfall boulders were  
259 modelled as rigid polyhedral. The source areas (i.e. volcanic rock) and remaining runout terrain  
260 types (i.e. loess and loess/volcanic colluvium) (Appendix 2, Table A1 and Figs. A1-A3) for  
261 the RAMMS model scenarios (i.e. RAMMS\_1, \_2, \_3) were chosen following the methods of  
262 Vick (2015) and Borella et al. (2016a) and delineated as polyline (Appendix 2, Figs. A2, A3)  
263 and polygon shapefiles (Appendix 2, Fig. A3) in ArcGIS from field observations, desktop study  
264 of orthophotography, and satellite imagery.

265

266 Boulder shape and size are highly influential in the dynamics and runout of a rockfall event  
267 (e.g. Leine et al., 2014; Latham et al., 2008). Boulder shapes and sizes used in the model  
268 simulations were representative of the true boulder geometries observed at Purau and Rapaki  
269 (Borella et al., 2016a). Rocks shapes were created using the RAMMS ‘rock builder’ tool, which  
270 creates boulder point clouds based on a user-defined shape and size. All boulder shapes  
271 reflected ‘real’ rock bodies that have been field-scanned. For each size class of boulder, varying  
272 shapes were selected, which are simplified to equant, flat, and long. Please see Supp.  
273 Information for more detail on boulder shape and size distributions utilized in each of the  
274 RAMMS modeling scenarios.

275

276 Vegetation was modelled in RAMMS as forest drag, a resisting force acting on the rock’s  
277 center of mass when located below the drag layer height. The forest was parameterized by a  
278 drag coefficient, effective up to the input height of the vegetation layer. Typical values for the  
279 drag coefficient range between 100 and 10,000 kg/s (Bartelt et al., 2013; Leine et al., 2014).



280 Vegetation was assigned an effective height of 10 m. A variable forest density was applied to  
281 account for the presumed denser vegetation (on average) within drainage valleys at the Purau  
282 study site (Appendix 2, Fig. A4). We assume more surface and subsurface water would be  
283 focused into topographic lows and would therefore promote denser tree growth. Within  
284 drainage valleys a uniform drag force of 6000 kg/s was applied to each of the simulated  
285 boulders. Elsewhere at the study site, a drag force of 3000 kg/s was applied. These forest values  
286 are equivalent to those utilized in Borella et al. (2016a) at Rapaki in the Port Hills of southern  
287 Christchurch. We also simulated a uniform forest density increase of 10000 kg/s (see Results).  
288 As evidenced by modern native forest analogs, tree growth was extended upward to the base  
289 of the source rock and was also applied to areas between outcropping volcanic source rock.

290

### 291 **3.4 Strong ground motions near rockfall source cliffs**

292

293 Strong ground motion accelerograms for stations LPCC, D13C, D15C, and GODS were  
294 obtained from GeoNet ([www.geonet.org.nz/](http://www.geonet.org.nz/), Fig. 6) to analyze the influence of ground motion  
295 on rockfalls. All these stations are Kinematics Etna instruments except LPCC, which is a  
296 CUSP-3 instrument. LPCC recorded both Mw 6.2 event on 2011-02-22 and Mw 6 event on  
297 2011-06-13. The other stations were installed following the Mw 6.2 earthquake and thus  
298 recorded only the Mw 6 earthquake. The data were sampled at 0.005 s (Nyquist frequency 100  
299 Hz) and filtered with an effective passband having corners ~0.05 Hz and ~40 Hz. We integrated  
300 accelerograms to produce velocity seismograms and computed envelopes using  $ENV = \sqrt{x(t)^2 + H(x(t))^2}$ ,  
301 where  $x(t)$  are time points in the seismogram and  $H$  is the Hilbert  
302 transform. The particle velocity hodograms are calculated in the horizontal plane by rotating  
303 the horizontal orthogonal components of the seismogram to a standard N-S E-W coordinate  
304 system. The time window of particle velocity hodograms is  $\pm 5$  s around the peak of the  
305 envelope of the east component. This ensures that the most significant ground motion resulting  
306 from both phase and group velocity peaks is accurately captured. Following a similar  
307 procedure, we computed particle motion hodograms by integrating accelerograms twice. These  
308 are given in Fig. 7 (A-E). Additional methods were used to analyze D13C data following  
309 interpretation of initial results; these are described in section 5.7.

310

## 311 **4 Results**

312

### 313 **4.1 Rockfall mapping and boulder frequencies**

314

#### 315 **4.1.1 Rapaki**

316

317 A comparison of the spatial distributions for pre-CES and CES rockfalls at Rapaki (Fig. 2)  
318 indicates that pre-CES rockfalls are more concentrated near the source area and have shorter  
319 maximum runout distances ( $560\pm 15$  m) than the furthest travelled CES rockfalls ( $700\pm 15$  m),  
320 that impacted Rapaki village during the 2011 Christchurch earthquakes. The CES rockfalls  
321 represent a subset of the pre-CES rockfall data set; the ratio of pre-CES ( $n=409$ ) to CES ( $n=49$ )  
322 rockfalls at Rapaki is  $\sim 8.5:1$  (Fig. 2). The pre-CES and CES rockfall data sets are separated  
323 into VB and CL boulders (Fig. 2, 4) to understand the influence of volcanic lithology on  
324 rockfall runout and final resting location. Very few CL boulders with volume  $\geq 1.0$  m<sup>3</sup> exist for  
325 pre-CES ( $n=18$ ) and CES ( $n=3$ ) rockfalls at Rapaki. Pre-CES and CES VB boulders display  
326 longer average and maximum runout distances than their CL counterparts (Fig. 2), and CES  
327 CL and VB boulders display longer average and maximum runout distances compared with  
328 their pre-CES equivalents. The ratio of pre-CES VB to CL and CES VB to CL rockfall boulders  
329 is  $\sim 22:1$  and  $\sim 15:1$ , respectively (Fig. 2).

330

#### 331 **4.1.2 Purau**

332

333 Pre-CES and CES rockfalls are widely distributed at the Purau study location (Fig. 3). Rockfall  
334 boulders are deposited on interfluves but are predominantly concentrated within nearby  
335 canyons, highlighting the strong influence of topography at the site (Fig. 3). Seven (7) CES  
336 detachment zones were identified in the field. CES rockfall boulders nearest to the Purau  
337 village display the longest runout distance (372 m) and most distinct spatial contrast with  
338 similarly sourced pre-CES boulders (deposited within  $\sim 105$  meters of the local volcanic source  
339 rock) (Fig. 3A). Elsewhere, pre-CES boulders can be observed at further distances from the  
340 source rock than CES rockfalls. The ratio of pre-CES to CES rockfall boulders is  $\sim 5:1$  (Fig.  
341 3A). Pre-CES VB boulders are deposited throughout the Purau location, while the deposition  
342 of CL pre-CES boulders is concentrated within the central and southern drainage canyons (Fig.  
343 6A). The ratio of pre-CES VB to CL boulders is  $\sim 2:1$  (Fig. 3B). CES VB boulders ( $n=127$ )  
344 significantly outnumber CL boulders ( $n=9$ ) at the Purau site (Fig. 3C), reflecting the lack of  
345 detachment within CL source rock lithologies during the CES. The ratio of CES VB to CL

346 rockfall boulders is ~14:1 and represents a significance difference compared with the  
347 corresponding pre-CES VB:CL ratio (Fig. 3C).

348

## 349 **4.2 Boulder morphology and other characteristics**

350

351 VB boulders (Fig. 4A-F) contain small to large porphyritic volcanic clasts that exhibit minor  
352 to moderate vesicularity (up to ~10%) and are embedded within a finer crystalline and ash-  
353 bearing matrix (see Fig. 4A,C,D,F). They are dominated by equant (all axes equal length)  
354 shapes (see Fig.4C) although elongate (two short axes, one long) forms are observed. Flat (one  
355 short, two long axes) morphologies are rare. VB pre-CES boulder surfaces show a high degree  
356 of weathering and surface roughness (Fig. 4A-D,F). The surface roughness results from in-situ  
357 differential weathering between the finer crystalline host matrix and more resistant embedded  
358 volcanic clasts (see Fig. 4D). Surfaces show deep pitting, with amplitudes often exceeding 5-  
359 10 centimeters in height. CL boulders (Fig. 4G-K) are more texturally homogenous, contain  
360 fewer vesicles (estimated ~<1%) and exhibit a higher relative density (Carey et al., 2014;  
361 Mukhtar, 2014). The pre-CES CL boulder surfaces exhibit low surface roughness (i.e. smooth  
362 compared with VB boulders). Elongate and flat boulder morphologies predominate for CL  
363 boulder lithologies (Fig. 4G-K).

364

365 Both VB and CL pre-CES boulders can be observed partially to nearly completely buried by  
366 loess-colluvium (see Fig. 4A,B,G). Instances do occur, however, where no sediment is built-  
367 up at the boulder backside (Fig. 4C) due to erosion (including tunnel gully formation). Burial  
368 in hillslope sediment is most common for boulders located on midslope and footslope positions,  
369 rather than those located on upper slope elevations, where erosion dominates. Pre-CES  
370 boulders located in drainage canyons are subject to rapid deposition and erosion, and therefore  
371 can be found without any sediment pile-up or preserving large colluvial wedges. VB boulders  
372 preserve the thickest colluvial wedge sediments (see Fig. 4B).

373

## 374 **4.3 Source rock characteristics**

375

376 **We combined high-resolution aerial photography (from UAV) with field observations to**  
377 **characterize the Rapaki source rock.** The volcanic source rock at Rapaki (Fig. 5A-C) and Purau  
378 (Fig. 5D,E) is comprised of interlayered VB and CL layers (Fig. 5A-E). The breccia layers  
379 comprise the bottom and top of discrete lava flows, while the coherent lava generally occupies

380 the center of the lava flow where cooling was not as rapid and there was less interaction with  
381 the substrate and/or cooling interface (Fig. 5C-G). Jointing is pervasive within the volcanic  
382 source rock, but to varying degree depending upon layer composition and corresponding  
383 texture. Layers comprised of CL exhibit the highest fracture density (Fig. 5E,F) and were  
384 formed during primary cooling of the lava flow, producing a columnar-style pattern. The CL  
385 layers contain numerous intersecting sub-vertical to vertical, to curvilinear joint sets, with  
386 spacing rarely exceeding ~1-2 m. The small joint spacing imparts a first-order control on CL  
387 boulder size and is reflected in the small size range for pre-CES CL boulders. Layers comprised  
388 of VB exhibit a lower fracture density, with joints more widely spaced (and irregular in shape),  
389 often 5-10 meters or greater apart (Fig. 5D,E). The wider spacing for joints within VB layers  
390 promotes greater rockfall boulder volume (see section 4.4. below).

391

392 During the CES, rockfall detachment occurred within approximately 9% (by area) of the  
393 volcanic source rock overlying the Rapaki study hillslope (Fig. 5A). The volcanic source rock  
394 is comprised of 86% VB and 14% CL (VB:CL ratio= $\sim$ 6:1). 69% of the CES detachment areas  
395 occurred within VB and the remaining 31% within CL (Fig. 5A). However, 20% of the  
396 identified CL source rock detached during the CES, while only 7% of the identified VB source  
397 rock detached during the CES, indicating the CL lithology was more susceptible to detachment.

398 ~~Due to its significant size and safety concerns, a similar characterization was not performed for~~  
399 ~~the Purau volcanic source rock.~~

400

401 ~~We were unable to conduct a source rock investigation at Purau with the same spatial resolution~~  
402 ~~as Rapaki because we considered the areal extent of the bedrock source cliffs to be too large at~~  
403 ~~Purau to address in this study and there were safety concerns relating to access and potential~~  
404 ~~for further rockfalls. However, some observations were made for the Purau source rock (Fig.~~  
405 ~~5D,E) as well as other volcanic coastal cliff outcrops at Sumner (Fig. 5F) and Red Cliffs (Fig.~~  
406 ~~5G). Field observations indicate that CL layers at Purau are not as prevalent as (and generally~~  
407 ~~thinner than) VB layers, but in some cases may exceed a thickness of 5 meters, which is thicker~~  
408 ~~than CL layers observed at Rapaki (see Fig. 5B,C). At Sumner and Redcliffs, VB and CL layers~~  
409 ~~display roughly equivalent thicknesses (~2-3 m), a condition not apparent at Rapaki or Purau.~~  
410 ~~The variability in layer thickness presumably reflects differences in proximity to source vents~~  
411 ~~and differing conditions during primary cooling of the lava flows.~~

412

413

#### 414 4.4 Boulder volume

415

416 The size and frequency-volume distributions for pre-CES and CES rockfall boulders (for  
417 volume  $\geq 1.0 \text{ m}^3$ ) at Rapaki and Purau display similarity (Fig. 8A,C) and can be modeled using  
418 power law functions (Fig. 8B,D), with the number of rockfall boulders decreasing significantly  
419 as volume increases. Overall, statistical coherence is observed at the 25<sup>th</sup>, median, and 75<sup>th</sup>  
420 percentile boulder sizes; however, pre-CES rockfalls are consistently higher for each of the  
421 size categories at the two study locations (Table 1). Rapaki displays the highest pre-CES to  
422 CES variance for 25<sup>th</sup>, median, and 75<sup>th</sup> percentiles, while Purau records the biggest pre-CES  
423 to CES variance for the average, 95<sup>th</sup> percentile, and maximum boulder volumes (Table 1, Figs.  
424 8A,C). **An inter-site comparison of rockfall volumes indicates that pre-CES rockfalls at Rapaki  
425 are greater for the 25<sup>th</sup>, median, and 75<sup>th</sup> percentile sizes (Table 1) while Purau exhibits larger  
426 sizes for the 95<sup>th</sup> percentile, maximum, and mean boulder categories (Table 1). For CES  
427 boulders, the 25<sup>th</sup>, median, 75<sup>th</sup>, and 95<sup>th</sup> percentile Rapaki CES boulders are slightly larger  
428 compared with Purau CES boulders, while the maximum and mean boulder size categories are  
429 higher at Purau (Table 1). Although differences are evident, the overall size distributions are  
430 comparable (Table 1).**

431

432 **The volume for pre-CES and CES VB boulders is significantly larger than the corresponding  
433 CL boulders at Rapaki (Fig. 8E, Table 2) and Purau (Fig 8F, Table 2). At Rapaki, VB pre-CES  
434 and CES boulder volumes display a similar trend (Fig. 8E) compared to the pre-CES and CES  
435 boulders (see Fig. 8A), indicating the dominance of VB boulders for volume  $\geq 1.0 \text{ m}^3$ . At  
436 Rapaki, pre-CES VB boulders display higher volumes (compared with CES VB boulders) in  
437 each of the size categories, particularly for median and maximum boulder sizes (Table 2). Pre-  
438 CES CL boulders display consistently higher values for each of the size categories with the  
439 exception of the 75<sup>th</sup> percentile (Fig. 8E, Table 2). At Purau, CES VB and CL boulders exhibit  
440 a smaller distribution of boulder sizes compared with their pre-CES equivalents (see Fig. 8F).  
441 Pre-CES VB and CL boulders are higher in each of the size categories (Table 2, Fig. 8F), with  
442 the exception of the median boulder size, where the CES CL median boulder volume is slightly  
443 more than the pre-CES CL value (Table 2). It is notable that the highest percent (%) variance  
444 in boulder volume between pre-CES and CES boulders is recorded for the Purau VB boulders  
445 (Table 2); the only exception is for maximum boulder size, where the percent (%) difference  
446 between Purau CL pre-CES and CES boulders is even greater (Table 2).**

447

448 The volume and frequency ratios for pre-CES and CES rockfall boulders are plotted in Figure  
449 9A. The pre-CES to CES boulder volume ratios at Rapaki and Purau range from ~8-12 and ~7-  
450 37, respectively (Table 3A, Fig. 9A). The corresponding frequency ratios are consistently  
451 lower, ranging from ~6-8.5 and ~3.5-27.5 (Table 3A, Fig. 9A). Overall, the boulder volume  
452 and frequency ratios are greater at Rapaki, with the exception of the CL lithology (Tables 3B,  
453 3A, and Fig. 9A).

454

455 The calculation of VB and CL boulder percentages at Rapaki for pre-CES and CES rockfalls  
456 indicates that VB boulders comprise  $\geq 98\%$  by volume and  $\geq 94\%$  by frequency (n) for all  
457 Rapaki conditions, while at Purau the corresponding percentages are  $\geq 90\%$  (volume) and  $\geq$   
458  $64\%$  (frequency), respectively (Table 3B). All of the lowest VB percentages exist at the Purau  
459 study location (see Table 3B, individual domain data).

460

#### 461 **4.5 Boulder runout distance**

462

463 The frequency-runout distance distribution for pre-CES boulders at Rapaki can be  
464 characterized by power and exponential laws (Fig. 9B), with the number of rockfall boulders  
465 with long runout distances decreasing dramatically with increasing distance from the volcanic  
466 source rock. The exponential regression is best fit to the entire data set (including extrapolated  
467 boulders within 100 m of source rock), while the power law displays the strongest fit for the  
468 mapped rockfall boulders (Fig. 9B). CES rockfalls display a poor exponential fit and do not  
469 indicate a similar inverse relationship between boulder frequency and runout distance (Fig.  
470 9B). The frequency-runout distribution for CES rockfalls indicates that the number of boulders  
471 remains more or less consistent regardless of distance from the source rock. Using the shadow  
472 angle method, we plot travel distance on the talus slope (Lt) versus height on the talus slope  
473 (Ht) with a fitted polynomial regression line (Fig. 9C). The correlation coefficient is 0.9699 for  
474 CES rockfalls and 0.9717 for pre-CES rockfalls (Fig. 9C). The minimum shadow angle for  
475 pre-CES is  $25^\circ$ , while the minimum shadow angle (for the furthest traveled CES rockfall  
476 boulders) is  $23^\circ$ . At Rapaki, the maximum runout distance for pre-CES and CES VB boulders  
477 exceeds the furthest travel distances for pre-CES and CES CL boulders, respectively (Table 4).  
478 The CES VB boulders exceed pre-CES VB runout by ~165 meters and CES CL boulders  
479 exceed CL pre-CES runout by ~138 meters (Fig. 2A,B; Table 4).

480

481 At Purau,  $Lt$  versus  $Ht$  is plotted for four (4) separate geomorphic domains (PD1-PD4) to  
482 evaluate the distribution of pre-CES and CES boulder runout distances (Fig. 9D; see Fig. 3 for  
483 domain locations). The pre-CES and CES rockfalls for the individual domain data sets are  
484 characterized by a variety of regression functions with high correlation coefficients (Fig. 9D;  
485 Supplementary Data, S24). CES rockfalls in PD1 and PD4 have significantly further maximum  
486 runout distances than their pre-CES counterparts, while the inverse is evident in PD2 and PD3.  
487 [We note that only two CES boulders were observed in PD2.] The minimum shadow angle for  
488 pre-CES rockfalls at Purau is  $25^\circ$ , while the corresponding minimum CES rockfall shadow  
489 angle is  $18^\circ$ . At Purau, the longest recorded runout distances occur for pre-CES CL and VB  
490 boulders and CES VB rockfall boulders within PD3 (Table 4).

491

492 At Rapaki, no relationship has been obtained plotting individual boulder volumes and the  
493 tangent of the shadow angle (Fig. 9E). A wide range of boulder sizes are evident for the full  
494 spectrum of pre-CES and CES rockfall runout distances by means of the shadow angle. The  
495 same is largely true at Purau, where correlations for the individual domains (PD1-PD4) are  
496 poor and the data has a high degree of scatter (i.e. low correlation coefficients); although the  
497 data does show a slight negative relationship between block volume and  $Ht/Lt$  ratio value (that  
498 is, a slight increase in runout distance as boulder size increases) (Fig. 9F).

499

## 500 **4.6 RAMMS rockfall modelling**

501

### 502 **4.6.1 RAMMS\_1**

503

504 Emplacement locations (Q 95%) are generated for simulated rockfalls released from the seven  
505 (7) field-identified CES detachment zones at Purau (labeled CES-1 through CES-7) (Fig. 10A).  
506 Observed CES boulder locations are depicted as red circles. RAMMS\_1 (bare-earth CES  
507 model scenario) is successful in replicating the overall spatial pattern for detached and  
508 distributed CES rockfalls at Purau for locations CES-3, -4, -5, -6, and -7. Below the CES-7  
509 source rock, RAMMS maximum runout distances ( $\sim 370$  m) are well matched to the maximum  
510 travel distance for mapped CES rockfalls ( $\sim 357$  m). Maximum runout distances for the  
511 RAMMS boulders are overestimated at CES-1 and CES-2 (Fig. 10A). We note that only 2  
512 boulders were released at CES-1 during the CES and were deposited within  $\sim 12$  meters of the  
513 source rock. RAMMS\_1 effectively captures the lateral dispersion for the mapped CES

514 boulders at CES-2, CES-3, and CES-4, but overestimates this effect within the CES-5 and CES-  
515 6 valleys, and slightly underestimates the lateral dispersion of CES rockfalls beneath CES-7.

516

#### 517 4.6.2 RAMMS\_2

518

519 The RAMMS\_2 model scenario (forested hillslope) is moderately successful (slight  
520 overprediction) in replicating the overall spatial distribution and maximum runout distances  
521 for the majority of mapped pre-CES rockfalls at Purau (Fig. 10B). The exception is area CES-  
522 7, where RAMMS predicts deposition of pre-CES boulders significantly farther (~325 m) from  
523 the source rock than is evident in the field (~80 m). Elsewhere, the greatest variance in  
524 maximum runout distance between RAMMS\_2 and the mapped pre-CES boulders is ~75-100  
525 m (see Fig. 10B). An increase in forest density to 10,000 kg/s, spread uniformly across the  
526 study site, produces the best fit to the pre-CES boulder spatial distributions (in particular,  
527 maximum runout distance) (see Figure 10B, white dashed line). RAMMS\_2 successfully  
528 models the lateral dispersion for the mapped pre-CES boulders (with the exception of area  
529 CES-7) (Fig. 10B). The RAMMS\_2 model scenarios identify pre-CES rockfall boulders that  
530 have likely experienced post-emplacment mobility (see Fig. 10B). Note the collection of pre-  
531 CES boulders within the central drainage canyon that exceed the limit of simulated RAMMS  
532 boulders (Fig. 10B). Field observations confirm that boulder depositional patterns beyond the  
533 limits of the final resting locations for RAMMS simulated rockfall boulders are consistent with  
534 deposition by debris flow and other transport/deposition processes. **This is further highlighted**  
535 **by the numerous and large pre-CES rafted boulders (maximum volume=20 m<sup>3</sup>) identified near**  
536 **the Purau coastline (see Fig. 3).** Importantly, we observe no mapped pre-CES boulders outside  
537 of the valleys that exceed the RAMMS\_2 simulated maximum runout distances.

538

#### 539 4.6.3 RAMMS\_3

540

541 RAMMS\_3 models the potential future rockfall hazard at Purau and assumes a bare-earth  
542 (deforested) hillslope and dry soil moisture conditions to insure a worst-case (conservative)  
543 outcome (Fig. 10C). As expected, RAMMS\_3 rockfalls obtain higher kinetic energy, velocity,  
544 and jump heights than RAMMS\_2 boulders (see Supplementary Data, S18, S19), and as a  
545 result, runout farther than the RAMMS\_2 boulders (Fig. 10B). On average, maximum runout  
546 distance for RAMMS\_3 boulders is ~450-500 m, representing an increase of ~100-150 m  
547 compared with RAMMS\_2 boulders, a difference consistent with results from RAMMS



548 numerical modeling at Rapaki (see Borella et al., 2016a). ~~The RAMMS\_3 results indicate that~~  
549 ~~the existing residence furthest to the north (S1) (Fig. 10C) and potential development at S2~~  
550 ~~could be adversely impacted by future rockfall events.~~ With the exception of area CES-7,  
551 RAMMS\_3 maximum runout distances are well in exceedance of the mapped locations for the  
552 CES rockfall boulders (Figs. 10A,C). ~~and highlights the potential input from additional~~  
553 ~~detachment sites within the Purau volcanic source rock.~~

554

#### 555 **4.7 Strong ground motion data**

556

557 High frequency data show complex velocity and displacement paths for any given site. The  
558 variations across the sites are significant, as reported previously (Van Houtte et al., 2012;  
559 Bradley, 2016). At the same site (LPCC, Fig. 7A,B), particle velocity and motion hodograms  
560 show different polarization characteristics for different earthquakes. Peak velocities and  
561 displacements recorded at LPCC site are higher for the Mw 6.2 than the smaller event Mw 6.0  
562 (Fig 7A, B). The observed inter-site and inter-event variations in polarization of peak velocities  
563 and displacements can be attributed to source radiation pattern (Lee, 2017) and complex wave  
564 propagation effects such as scattering. For instance, simulating high frequency (> 1 Hz) 3-D  
565 wavefields, Takemura et al. (2015) showed that near-station irregular topography amplifies  
566 scattering of seismic wavefield, producing long coda and distortions to P wave polarizations.  
567 This is not surprising given that Fresnel volume – the region to which a transmitting seismic  
568 wave is sensitive – is inversely related to wave frequency (Spetzler and Snieder, 2004), due to  
569 which near-station geological conditions modify wave characteristics at high frequencies. The  
570 control of near-station geology over polarization and amplification characteristics at high  
571 frequencies (Bouchon & Barker, 1996) reduces our ability to extrapolate these characteristics  
572 to distant sites.

573

### 574 **5 Discussion**

575

#### 576 **5.1 Rockfall spatial distributions and frequencies**

577

578 At Rapaki, significant differences in spatial distribution between the pre-CES and CES boulder  
579 populations are observed (Fig. 2 and Table 4). The increased distance for the CES rockfall  
580 boulders is interpreted as an effect of anthropogenic deforestation on the hosting hillslope,  
581 which enabled CES boulders to travel further than their pre-CES counterparts due to reduced

582 resistance from vegetation (Borella et al., 2016a). The increase in CES runout distance  
583 (~165±15 m) and corresponding reduction in minimum shadow angle resulted in significant  
584 impact and damage to homes and infrastructure in the Rapaki village, highlighting the  
585 importance of considering the effects that modifications to hillslopes may have on rockfall  
586 hazard. At Rapaki, pre-CES VB boulders are present in significantly greater number and have  
587 further average and maximum runout distances than the pre-CES CL boulder lithologies (Fig.  
588 2A, Table 4). A similar relationship is evident between the CES VB and CL boulders, where  
589 CES boulders with the furthest runout distances are exclusively comprised of volcanic breccia  
590 (Fig. 2B). It is possible that the reduced runout distances for pre-CES and CES CL boulders is  
591 a statistical counting bias (i.e. low number of CL boulders for volume  $\geq 1.0 \text{ m}^3$ ), but a more  
592 plausible explanation is that the reduced runout distance for CL boulder lithologies is a result  
593 of CL boulder shapes being dominated by elongate and flat morphologies (Fig. 10A-F), which  
594 would have more difficulty traveling downslope.

595

596 At Purau, discerning the differences in spatial distribution between pre-CES and CES rockfalls  
597 is more difficult, primarily due to the topographic forcing of rockfalls into nearby drainage  
598 valleys and post-emplacment mobilization (Fig. 3). Location CES-7 (furthest southern  
599 rockfalls) does show a similar pre-CES:CES spatial scenario to Rapaki, with CES boulders  
600 traveling significantly further than their pre-CES equivalents (see Fig. 5); a discrepancy which  
601 could also be attributed to intervening deforestation on the hillslope. However, elsewhere at  
602 the Purau field site inverse spatial scenarios are evident, with pre-CES boulders deposited  
603 further from the source rock than their CES counterparts (see Fig. 2A, Table 4). This is  
604 primarily observed within drainage valleys where field observations suggest pre-CES boulders  
605 have been remobilized (debris flows, floods) and carried further from the source rock following  
606 their initial emplacement.

607

608 The CES rockfall boulders at both sites represent a subset of the larger pre-CES rockfall  
609 database, suggesting the preservation of multiple pre-CES rockfall events. The ratio for the  
610 number of pre-CES to CES rockfall boulders is higher at Rapaki (~8.5:1) than Purau (~5:1)  
611 (Table 3, Figs. 2, 3). One cause of the observed difference may be the higher number of CL  
612 boulders with size  $\geq 1.0 \text{ m}^3$  at the Purau study site (Fig. 8E,F). At Rapaki, most of the  
613 detachment within the CL source rock generated boulder volumes below the  $1.0 \text{ m}^3$  threshold.  
614 As a result, the ratio of pre-CES VB:CL boulders is significantly higher at Rapaki (~22:1)

615 (Table 3B, Fig. 2A) than Purau (~2:1) (Table 3B, Fig. 3B). This contrasts with the ratio of CES  
616 VB:CL boulders at Rapaki (~15:1) (Table 3B, Fig. 2B) which shows near equivalence to Purau  
617 (~14:1) (Fig. 3C). The CES VB:CL ratio at Purau is more consistent with our field observations  
618 where VB predominates in the source rock. Overall, the results indicate there is a high degree  
619 of variability for lithology and discontinuity spacing (e.g. joints) within the source rock and  
620 suggests the cumulative ratio of VB:CL boulders can be significantly different from that  
621 generated locally during a single rockfall event.

622

## 623 **5.2 Boulder morphology and other characteristics**

624

625 ~~It is well established that boulder morphology (shape) plays a primary role in the spatial~~  
626 ~~distribution of the rockfalls (e.g. Leine et al., 2014).~~ The shapes for the VB (Fig. 4A-E) and  
627 CL (Fig. 4G-K) boulders are primarily controlled by pre-existing discontinuities (primarily  
628 joints) in the source rock. We modeled the influence of boulder shape on spatial distribution  
629 for the VB and CL lithologies assuming detachment from the CES-7 site (under bare-earth  
630 conditions) using RAMMS (Fig. 11). To eliminate the effect of boulder size, a volume of 1.0  
631 m<sup>3</sup> was assumed for all rockfall boulders. The VB boulders were assigned a range of equant  
632 boulder shapes, while CL boulders were assigned only elongate and flat boulder morphologies.  
633 The model results highlight the differences in boulder spatial distribution resulting from  
634 differences in boulder shape, with equant (VB) boulder lithologies displaying a significantly  
635 higher relative percentage of longer runout distances (Fig. 11A) compared with the  
636 elongate/flat (CL) boulder morphologies (Fig. 11B). We recognize that the modeling represents  
637 an ideal scenario (i.e. other transition morphologies do exist for the VB and CL boulders) and  
638 was conducted primarily to provide a sense for the expected spatial patterns assuming the  
639 distinct VB and CL boulder shapes. Further work is required to verify coherence between field  
640 observations and model results.

641

## 642 **5.3 Source rock characteristics**

643

644 ~~We combined high resolution aerial photography (from UAV) with field observations to~~  
645 ~~characterize the Rapaki source rock. The VB and CL percentages in the Rapaki source rock~~  
646 ~~(86% VB and 14% CL) are lower than the corresponding VB and CL percentages determined~~  
647 ~~from rockfall frequency and volume for the pre-CES (96% VB and 4% CL) and CES (94% VB~~  
648 ~~and 6% CL) rockfalls. We attribute the percent differences between source rock and rockfalls~~

649 to the influence of the larger VB boulder sizes and the lower number of CL rockfalls meeting  
650 the  $\geq 1.0 \text{ m}^3$  size threshold. These two factors also explain detachment during the CES, where  
651 69% of the detachment areas occurred within VB and the remaining 31% within CL (Fig. 5A-  
652 C), yielding a lower VB:CL ratio of  $\sim 2:1$  compared with the corresponding boulder volume  
653 and frequency ratios ( $\sim 15:1$  and  $\sim 52:1$ , respectively) (Table 3B). ~~Comparisons between~~  
654 ~~volcanic source rock characteristics and boulder volumes (VB and CL) are discussed in Section~~  
655 ~~5.4. (see below).~~

656

~~We were unable to conduct a similar source rock investigation at Purau because the size of the~~  
657 ~~source rock was too great and in several cases deposition of rockfall boulders into discrete~~  
658 ~~geomorphic domains resulted from detachment on multiple source rock outcrops. However,~~  
659 ~~observations were made for the Purau source rock (Fig. 5D,E) as well as other volcanic coastal~~  
660 ~~cliff outcrops at Sumner (Fig. 5F) and Red Cliffs (Fig. 5G). Field observations indicate CL~~  
661 ~~layers at Purau are not as prevalent as (and generally thinner than) VB layers, but in some cases~~  
662 ~~may exceed a thickness of 5 meters, which is thicker than CL layers observed at Rapaki (see~~  
663 ~~Fig. 5B,C). At Sumner and Redcliffs, VB and CL layers display roughly equivalent thicknesses~~  
664 ~~( $\sim 2\text{--}3 \text{ m}$ ), a condition not apparent at Rapaki or Purau. The variability in layer thickness~~  
665 ~~presumably reflects differences in proximity to source vents and differing conditions during~~  
666 ~~primary cooling of the lava flows.~~

668

#### 669 **5.4 Boulder volume**

670

671 The size and frequency-volume distributions for pre-CES and CES rockfalls at the two study  
672 sites can be modeled using a power law (Figs. 8A-D); ~~and indicate a predictable decrease in~~  
673 ~~the number of boulders as boulder volume increases.~~ a relationship that is well-established (e.g.  
674 Dussauge-Peisser et al., 2002; Guzzetti et al., 2002) for rockfalls globally and has also been  
675 successfully applied for CES rockfalls in Banks Peninsula (Massey et al., 2014). ~~At both study~~  
676 ~~locations, pre-CES rockfalls exceed the size of their CES counterparts in all statistical~~  
677 ~~categories (Table 1).~~ The net increase in volume distribution for pre-CES boulders could  
678 represent a statistical effect and reflect the inclusion of more boulders into the rockfall data set  
679 through time (which would increase the likelihood of more large boulders) and/or could reflect  
680 higher shaking intensities and/or source rock vulnerability during pre-CES events. ~~A~~  
681 ~~comparison of rockfall volumes between the two sites indicates that pre-CES rockfalls at~~

682 Rapaki are greater for the 25<sup>th</sup>, median, and 75<sup>th</sup> percentile sizes (Table 1) while Purau exhibits  
683 larger sizes for the 95<sup>th</sup> percentile, maximum, and mean boulder categories (Table 1). For CES  
684 boulders, the 25<sup>th</sup>, median, 75<sup>th</sup>, and 95<sup>th</sup> percentile Rapaki CES boulders are slightly larger  
685 compared with Purau CES boulders, while the maximum and mean boulder size categories are  
686 higher at Purau (Table 1). Although differences are evident, the overall size distributions are  
687 comparable (Table 1). Variations in CES vs. pre-CES boulder volumetric distributions for the  
688 same lithologies could reflect structural and/or more subtle lithologic variability within the  
689 source cliffs from which boulders were derived, and/or post-detachment weathering during  
690 boulder transport or *in situ*. The significantly higher volumes for VB boulders (pre-CES and  
691 CES) at both study sites reflects the predominance of VB within the source rock and wider  
692 joint spacing within the thicker VB layers. As expected, the pre-CES VB and CL boulder sizes  
693 exceed those of their CES equivalents, with the exception of the 75<sup>th</sup> percentile CL boulders at  
694 Rapaki and median CL boulders at Purau (Table 2, Figs. 8E,F). It is notable that the largest  
695 percent variance between pre-CES and CES boulder size occurs for the Purau VB boulders  
696 (with the exception of maximum boulder size) (Table 2). We are uncertain why this difference  
697 is greatest within the Purau VB boulders, but could reflect a smaller joint spacing at the CES  
698 VB detachment sites.

699

## 700 5.5 Boulder runout distance

701

702 The frequency runout distance distribution for pre-CES boulders at Rapaki can be modeled  
703 using a power law and exponential fit. The exponential law fit (Fig. 9B, short dashed line)  
704 includes all data points (including extrapolated data within 100 m of source rock) and for CES  
705 boulders highlights the importance of slope and initial impact velocity at the cliff base, which  
706 causes more boulders to be deposited at greater distances and creates a deviation from the  
707 power law fit (Fig. 9B, solid line). The exponential fit for CES rockfall boulders is poor and  
708 indicates there is no discernable correlation between CES boulder frequency and runout  
709 distance (Fig. 9B, long dashed line). Despite the low number of CES boulders (n=48), it is  
710 interesting that the CES runout distribution shows such a noticeable deviation from the pre-  
711 CES data set and could reflect the influence of deforestation on runout distance. This would  
712 imply that the incremental input of CES and future rockfalls at Rapaki (emplaced during bare-  
713 earth conditions) will modify the overall trend for the cumulative rockfall data set.

714

715 At Rapaki, the shadow-angle  $Ht/Lt$  relationship is fit best using a polynomial regression (Fig.  
716 9C). The trend indicates a positive correlation between talus slope height ( $Ht$ ) and travel  
717 distance on the talus slope ( $Lt$ ), with a reduction in the rate of increase as rockfall runout ( $Lt$ )  
718 increases. At Purau, CES and pre-CES rockfalls (within individual geomorphic domains) are  
719 modeled using a variety of data functions (e.g. linear, log, polynomial), suggesting intra-site  
720 geomorphic and geologic factors affecting rockfall hazard are spatially variable (Fig. 9D). We  
721 note that Copons (2009) reports linear regression lines for historical rockfalls in the Central  
722 Pyrenees using the shadow-angle method, and locally, Massey et al. (2014) also show linear  
723 regression fits using the shadow-angle method for CES rockfalls in the Port Hills of southern  
724 Christchurch. Our data indicates that non-linear regression functions (for the shadow-angle  
725 method) are more successful in capturing the  $Ht/Lt$  relationship as distance from the source  
726 rock increases. ~~No clear relationship is obtained between boulder volume and runout distance~~  
727 ~~at Rapaki (Fig. 9E) and Purau (Fig. 9F)~~. At both sites, a wide range of boulder sizes exist for  
728 the full spectrum of pre-CES and CES  $Ht/Lt$  ratios, suggesting that boulder size is not a primary  
729 driver for runout distance at the study sites; although it is possible that smaller boulders (e.g.  
730  $\sim 1\text{-}2\text{ m}^3$ ) exhibiting long runout distances (i.e. low  $Ht/Lt$  ratios) may represent smaller rock  
731 fragments detached from larger boulders during transport and eventual emplacement on the  
732 hillslopes and within valleys.

733

## 734 **5.6 RAMMS rockfall modelling**

735

### 736 **5.6.1 RAMMS\_1**

737

738 A primary challenge in replicating the distribution of CES rockfalls was determining an  
739 appropriate set of terrain parameters for the drainage valleys (see Appendix 1, Table A1). To  
740 match the RAMMS boulders with the field-mapped CES rockfalls (Fig. 10A) it was necessary  
741 to create separate valley terrain polygons and modify the terrain parameters to reflect the high  
742 degree of impedance and/or dampening (Vick et al., 2019) in the drainage gullies (see  
743 Appendix 2, Table A1). Our field observations confirm the presence of abundant pre-existing  
744 boulders within drainage valleys (Fig. 12A-F) and many instances where CES boulders were  
745 stopped by pre-CES rockfalls (see Fig. 12A-C). The effect of pre-CES rockfall debris on  
746 boulder transport and final resting location needs to be further investigated in order to  
747 effectively model impediments within drainage valleys. Further, a more refined understanding  
748 of the influence that substrate soil moisture content has on rockfall runout is required (Vick et

749 al., 2019). We note that the DEM used for our study has a resolution of 4 m and may not  
750 adequately simulate the smaller scale surface roughness (e.g. clustering of boulders below this  
751 size threshold) observed during our field studies (Fig. 12A-G).

752

### 753 5.6.2 RAMMS\_2

754

755 ~~The RAMMS\_2 model scenario (prehistoric/forested hillslope) is moderately successful (slight~~  
756 ~~overprediction) in replicating the overall spatial distribution (including maximum runout~~  
757 ~~distances) for the majority of mapped pre-CES rockfalls at Purau (Figs. 10B).~~ The best  
758 RAMMS\_2 model fit occurs when the forest density is increased (to 10,000 kg/s) (~~dense~~  
759 ~~vegetation~~) and applied uniformly across the Purau hillslopes (see Figure 10B, white dashed  
760 line). This represents an increase compared with the forest density used at Rapaki (i.e. 3000  
761 kg/s for moderate vegetation [interfluves], 6000 kg/s for dense vegetation [valleys] (see Borella  
762 et al., 2016a) and implies that vegetation may have been denser on the northwest-facing Purau  
763 hillslopes compared with the south/southeast facing Rapaki hillslope.

764

765 We note the difference between maximum runout distance for RAMMS and empirical pre-  
766 CES boulders at the CES-7 site (Fig. 10B). ~~RAMMS predicts that pre-CES boulders should be~~  
767 ~~deposited further from the source rock (maximum runout distance ~ 325 m) than is observed~~  
768 ~~(maximum runout distance ~ 105 m) in the field.~~ Several possible explanations exist including:  
769 (1) pre-CES boulders were in fact deposited further from the source rock and were  
770 subsequently buried by loess and hillslope colluvium; (2) RAMMS underestimates the effect  
771 of hillslope vegetation at Purau during prehistoric times; (3) during pre-CES times less of the  
772 source rock was exposed (due to burial) and therefore the volcanic rock was less susceptible to  
773 detachment during shaking; and/or (4) during pre-CES shaking events the direction of strong  
774 ground motion was not favorable to rockfall detachment. Scenario 1 is possible but would need  
775 to be confirmed through subsurface trenching or ground penetrating radar (GPR) methods.  
776 Tunnel gully erosion has exposed sections of the subsurface on the CES-7 hillslope and no  
777 buried boulders are evident. Scenario 2 is probable based on our observations of forested  
778 hillslopes elsewhere in the Port Hills and greater Banks Peninsula area. It is common for dense  
779 native vegetation to grow up to, and in some cases, onto portions of the volcanic source rock.  
780 In these cases, a high volume of detached rockfalls are stopped adjacent to the source rock and  
781 never generate the required momentum to runout an appreciable distance. Scenario 3 is also a  
782 possibility and requires that the CES-7 source rock was partially buried during emplacement

783 of the pre-CES rockfalls. The last phase of hillslope aggradation would have occurred during  
784 the last glacial maximum (~18-24 ka) and possibly up to ~12-13 ka (see Borella et al., 2016b).  
785 We assume the Purau hillslopes have been net erosional (i.e. downwasting) since the early  
786 Holocene; a condition that would have been significantly accelerated after deforestation in the  
787 Purau area. Option 4 is a final possibility but would require that the ~north facing PD1 source  
788 rock is oriented in such a way that strong ground motions from multiple prehistoric shaking  
789 events were unable to create rockfall detachment to the degree evident in the CES (see section  
790 5.7 for more discussion on strong ground motions).

791

792 RAMMS 2 model scenarios effectively identify pre-CES rockfall boulders that have likely  
793 experience post-emplacement mobility (Fig. 10B). This is shown by the collection of pre-CES  
794 boulders within the central drainage canyon that exceed the limit of simulated RAMMS  
795 boulders (Fig. 10B), indicating a transport mechanism other than rockfall. ~~Field observations~~  
796 ~~confirm that the depositional patterns of boulders located beyond the limits of what RAMMS~~  
797 ~~predicts are consistent with debris flow and other transport/deposition processes. This is further~~  
798 ~~highlighted by the numerous and large pre-CES rafted boulders (maximum volume=20 m<sup>3</sup>)~~  
799 ~~identified near the Purau coastline (see Fig. 3).~~ This result has implications for rockfall hazard  
800 studies because boulder locations not reflective of cliff detachment and subsequent downslope  
801 displacement by bouncing, sliding, and rolling (that is, rockfall) should be excluded from any  
802 data set before assessing the potential rockfall hazard and associated risk. Furthermore,  
803 paleoseismic studies attempting to determine the timing and recurrence interval of prehistoric  
804 rockfall events should avoid using boulders with complex post-emplacement mobility  
805 histories.

806

807 The absence of any pre-CES boulders exceeding the RAMMS\_2 maximum runout distance  
808 (with the exception of rockfalls within valleys) (Fig. 10B) implies that the mapped pre-existing  
809 boulders ~~(yellow circles)~~ were deposited prior to deforestation of the Purau hillslopes and are  
810 prehistoric (i.e. deposited prior to European arrival) in age. This result is consistent with  
811 prehistoric boulder ages determined at the Rapaki study site where the youngest emplacement  
812 ages for pre-CES boulders are ~2-6 ka (Mackey and Quigley, 2014; Borella et al., 2016b).

813

### 814 5.6.3 RAMMS\_3

815



816 ~~With the exception of area CES-7, RAMMS\_3 maximum runout distances are well in~~  
817 ~~exceedance of the mapped locations for the CES rockfall boulders (Fig. 10C), and RAMMS\_3~~  
818 highlights the increased spatial extent (including maximum runout distance) of rockfalls that  
819 could result from more widespread detachment within the Purau source rock, particularly for  
820 detachment sites overlying hillslopes where boulder trajectories are not as strongly influenced  
821 (i.e. captured) by nearby valleys. Although we caution against using RAMMS\_3 as a rockfall  
822 hazard map, the model results do provide a first-order indicator of low-lying areas that are most  
823 susceptible to future rockfall hazard and suggest that development at the S1 and S2 sites could  
824 be adversely impacted by future rockfall events (Fig. 10C). Assuming terrain characteristics  
825 remain similar, Sites 3, 4, and 5 are unlikely to be impacted by rockfall boulders in the future,  
826 although additional mapping and related structural studies of the volcanic source rock is  
827 required to determine the most vulnerable rockfall source areas.

828

## 829 **5.7 Interpretations of strong ground motion data**

830

831 Preceding studies provide some insight into possible strong ground motion characteristics at  
832 Rapaki and Purau during the Mw 6.0 and 6.2 earthquakes. Kaiser et al.'s (2014) seismic array  
833 analysis of weak ground motion provides information regarding frequency-dependent  
834 amplification at Kinsey Terrace, Redcliffs, and Mt. Pleasant (henceforth Ksites), all of which  
835 are north-facing slopes in the Port Hills. They found that both morphological features as well  
836 as properties of the wave propagation media control frequency-dependent amplification.  
837 Significant ground motion amplification was observed at 1 – 3 Hz frequency range on top of  
838 narrow, steep-sided ridges. At these low frequencies ( $f$ ), seismic wavelengths ( $\lambda$ ) are  
839 comparable to ridge width of Ksites. Therefore, seismic waves in the 1 – 3 Hz frequency band  
840 appear to excite natural resonance (or natural frequency;  $f_n$ ), optimizing ground motion.

841

842 It is interesting to evaluate the implications of Kaiser et al.'s (2014) low frequency observations  
843 to Rapaki and Purau rockfall sites. Both these sites are located at higher elevations than Ksites.  
844 Thus, their ridge width (~400 – 500 m) is somewhat less than that at Ksites (~ 600 – 1000 m).  
845 Using this information, we estimate  $f_n$  to be  $< 5$  Hz (see Supp. Info.).

846

847 Whether ground motion with  $f_n$  was excited at these sites depends on the amount of energy  
848 carried by seismic waves in that frequency band. This information is contained in the spectra

849 of velocity seismograms – a proxy for kinetic energy distribution over frequency. We selected  
850 D13C station for this preliminary analysis because the distance between this station and the  
851 Rapaki site is only about 2 km. They are also at similar elevations with ridge morphologies  
852 resembling each other. Rapid variations in geological conditions are unlikely over such short  
853 length-scales, which allows us to extrapolate both high and low frequency wave characteristics  
854 observed at D13C station to Rapaki with less uncertainty than the other stations. The nearest  
855 station to Purau is LPCC (~ 5 km). The two sites are vastly different as LPCC is located at the  
856 toe of a steep cliff in the Lyttelton Port, whereas Purau sites are high elevation ridges. Thus,  
857 ground motion recorded at LPCC is not a reliable proxy for ground motion characteristics at  
858 Purau. The next nearest station D15C is ~ 7 km from Purau and it suffers from morphological  
859 dissimilarities (variations in ridgeline orientation and morphology) that make extrapolating  
860 ground motion between the sites highly unreliable. Although the D13C station is located ~10  
861 km from Purau, the similarity of morphological features including elevation makes D13C a  
862 desirable station to understand ground motion at Purau.

863

864 We computed velocity spectra of east and north components of the station D13C (Fig. 13) to  
865 qualitatively assess seismic energy transmission through our rockfall sites. We find that the  
866 transition from the flat spectrum to a rapid fall off occurs at ~3 – 4 Hz. This means that the 13  
867 June 2011 Mw 6 earthquake carried most of its energy at frequencies less than ~3 – 4 Hz.  
868 Together with our estimates of  $f_n$  (< 5 Hz), we can thus infer that the passage of seismic waves  
869 excited natural resonance at Rapaki and Purau sites. The combined effects of natural resonance  
870 and wave focusing towards the ridge crest (Hartzell et al., 1994; Bouchon & Barker, 1996) in  
871 these hard rock sites have the potential to optimize shaking, promoting rockfalls.

872

873 It is interesting to note, however, that D13C recorded the lowest peak velocities (223 mm/s and  
874 178 mm/s) and displacements (38 mm and 74 mm) of the four stations considered here (Fig.  
875 7C). Out of these stations, it is also the only station that recorded no acceleration above 0.3g  
876 on any component. These features of the wavefield are not surprising because distance from  
877 D13 C to epicentre of the Mw 6 earthquake is twice (~9 km) as large as that from the other  
878 stations (~4.5 km). For this reason, it is likely that other possible effects (e.g., rockmass  
879 weakening by prior CES earthquakes), in addition to strong ground motions from the Mw 6  
880 earthquake, were responsible for triggering major rockfalls at the study sites. Unfortunately,  
881 D13C was not in operation at the time of these previous larger earthquakes to assess severity  
882 of ground motion. Nonetheless, records from stations closest to D13C indicate that those sites

883 have exceeded the 0.3g peak ground acceleration (PGA) threshold important for engineering  
884 considerations. For instance, LPCC station located ~6 km from D13C recorded 0.3g and 0.9g  
885 PGA following the Mw 7.1 and Mw 6.2 events respectively (Bradley & Cubrinovski, 2011).  
886 Moreover, extrapolation of PGA contours of Bradley (2012) suggests that D13C and Rapaki  
887 sites experienced PGAs exceeding 0.25g and 0.45g during Mw 7.1 and Mw 6.2 earthquakes  
888 respectively. Some of the rockfall sites investigated herein might have had reached a critical  
889 failure threshold prior to being triggered by the 13 June 2011 Mw 6 earthquake.

890

891 Particle velocity and motion hodograms (Fig. 7A-E) also carry directional information of  
892 particle behavior in addition to intensity. Past studies show that seismic wave polarizations are  
893 amplified in directions perpendicular to fracture surfaces, weakening the coherence between  
894 outer blocks of rock with bedrock during the passage of a seismic wave (Kleinbrod et al., 2017;  
895 Burjánek et al., 2018). If blocks of rock are primed for failure by previous events, this effect  
896 can produce rockfalls in earthquakes as small as local magnitude 4.0 (Keefer, 1984). The  
897 velocity hodogram of D13C exhibits a strong ENE-WSW component. Note that this direction  
898 makes roughly ~30° to ~60° angle with rock faces at PD2, PD3, PD4, and RAP sites (Fig. 7C).  
899 Thus, it is reasonable to assume that particle velocities in this dominant direction are favorable  
900 for triggering rockfalls particularly if the rock faces were primed for failure. The angle between  
901 this dominant velocity component and the rock face at PD1 site, however, appears to be less  
902 than ~20° and possibly is not as favorable for triggering rockfalls as for other sites. On the other  
903 hand, the particle motion hodogram has two dominant directions; WNW and WSW. Depending  
904 on the strike of the rock face, either one of these directions can orient particle motion favorably  
905 for rockfalls. For instance, site RAP has a rock face strike of 25°, which is sub-parallel to the  
906 WSW particle motion direction. However, the WNW particle motion direction makes a steep  
907 angle with the rock face and thus can promote rockfalls. Combining information from particle  
908 velocity and motion hodograms, we hypothesize that directional aspects were favorable to  
909 rockfall triggering at the Rapaki and Purau sites.

910

## 911 **5.8 Pre-existing rockfalls as predictive database**

912

913 Our study indicates that pre-existing rockfalls provide an accurate range of expected boulder  
914 volumes, shapes, and % lithologic variance (i.e. VB vs CL) **but their use as a spatial indicator**  
915 **for future rockfalls should be approached with caution because there are a variety of geologic**  
916 **and anthropogenic factors that influence the final resting location for rockfalls. These factors**

917 include changes to the rockfall source (i.e. emergence of bedrock sources from beneath  
918 sedimentary cover), remobilization of prior rockfalls by surface processes including debris  
919 flow transport, collisional impedance with pre-existing boulders, potential natural and human-  
920 induced landscape changes (including deforestation), and variations in the location, size, and  
921 strong ground motion characteristics of past rockfall-triggering earthquakes. Our study  
922 indicates that pre-CES rockfalls underestimated the expected average and maximum runout  
923 distances on interfluves, in part, because pre-CES rockfalls were probably emplaced on a  
924 forested hillslope. Conversely, the locations for pre-CES boulders in well-established drainage  
925 valleys/channels may overestimate the expected runout for future rockfalls because the  
926 rockfalls have been remobilized after their initial emplacement.

927

928 Prior to the CES, rockfall hazard was not considered a major risk in Banks Peninsula and  
929 surrounding areas (Townsend and Rosser, 2012), including the Port Hills of southern  
930 Christchurch, where damage was most critical and 5 fatalities occurred (Massey et al., 2014).  
931 To date, we are aware of only four studies that have dated pre-CES rockfalls in Banks Peninsula  
932 (Mackey and Quigley, 2014; Borella et al., 2016b, Sohpati et al., 2016; Litchfield et al., 2016),  
933 and all of these investigations were undertaken after the CES. We assume this was primarily  
934 because there were few records of historical rockfall occurrence, and of those described  
935 (Lundy, 1995), none hinted at the potential for future widespread cliff collapse and rockfall in  
936 the region. However, the geologic record (i.e. prehistoric rockfalls) provides evidence that  
937 rockfall events of similar magnitude (or greater) have occurred in the past. In regions devoid  
938 of historical or contemporary rockfalls, pre-existing rockfalls represent the only empirical  
939 proxy for evaluating local rockfall behavior and provide valuable input for rockfall modeling  
940 and risk assessment studies. Existing rockfalls provide important data for predicting rockfall  
941 volumetric, lithologic, and morphologic (i.e. boulder shape) characteristics, but a thorough  
942 consideration of landscape evolutionary chronologies (including deforestation) and post-  
943 emplacement mobility scenarios is required before pre-existing rockfalls can be confidently  
944 used as future spatial indicators.

945

## 946 **6 Conclusions**

947

948 The spatial distributions and physical-geological properties of individual (n=1093) rockfall  
949 boulders deposited at two sites in Banks Peninsula prior to the 2010-2011 Canterbury  
950 earthquake sequence (CES) are compared to boulders (n=185) deposited during the CES. Pre-

951 CES to CES boulder ratios range between ~5:1 and 8.5:1 respectively, suggesting preservation  
952 of multiple pre-CES rockfall events with a flux analogous to or smaller than CES events, and/or  
953 pre-CES event(s) of larger flux. Pre-CES and CES boulders at one site (Purau site) have  
954 statistically-consistent power-law frequency-volume distributions between 1.0 to >100.0 m<sup>3</sup>.  
955 At the Rapaki site, CES boulders have smaller and more clustered volumetric distributions that  
956 are less well fit by power-laws compared with the pre-CES data, interpreted to reflect variations  
957 in rockfall source characteristics through time. Boulders of volcanic breccia (VB) have a larger  
958 binned-percentage of large volume boulders and more equant boulder aspects relative to  
959 coherent lava (CL) boulder lithologies at both sites, revealing lithologic controls on rockfall  
960 physical properties. The maximum runout distances for Rapaki CES VB and CL boulders are  
961 greater than that of pre-CES boulders of equivalent lithologies, volumes and morphologies.  
962 This is interpreted as an effect of anthropogenic deforestation on the hosting hillslope, which  
963 enabled CES boulders to travel further than their pre-CES counterparts due to reduced  
964 resistance from vegetation. At Purau, isolated geomorphic domains exhibit this same effect,  
965 however in other intra-site locations, pre-CES boulder locations exceed runout distances of  
966 CES boulders. This is interpreted to reflect post-depositional mobility of prehistoric boulders  
967 via debris flows and other surface processes, reduction of CES boulder runouts in channels due  
968 to collisional impedance from pre-CES boulders, and heterogeneity in the CES boulder  
969 distributions, which reduced the likelihood of large runout boulders occurring due to smaller  
970 volumetric fluxes. The shadow angle method is a reliable predictor for pre-CES and CES  
971 rockfall runout at both sites. At Rapaki, the pre-CES and CES rockfall data is best fit using a  
972 2<sup>nd</sup> order polynomial regression, while at Purau rockfalls require a variety of data fits (e.g.  
973 linear, log, polynomial), suggesting intra-site geomorphic and geologic factors affecting  
974 rockfall hazard are spatially variable. Bare-earth and forested numerical modeling suggest that  
975 the majority of pre-CES rockfalls were emplaced before deforestation of the Purau hillslopes  
976 and enables identification of boulder sub-populations that have likely experienced post-  
977 emplacement mobility. [The RAMMS\\_3 model effectively shows the potential spatial extent of  
978 rockfalls that could result from more widespread detachment within the Purau source rock and  
979 provides a preliminary indicator of low-lying areas most susceptible to future rockfall hazard.  
980 More in-depth rockfall hazard analyses \(including numerical rockfall modeling\) are required  
981 at Purau and should consider the implementation of boulder morphologies, terrain parameters,  
982 and hillslope vegetation attributes developed in this study.](#) Our research highlights the  
983 challenges of using rockfall distributions to characterize future rockfall hazards in the context

984 of geologic and geomorphic variations, including natural and anthropogenically-influenced  
985 landscape changes.

986

987 *Acknowledgements*

988

989 Financial support for the project came from the New Zealand Earthquake Commission  
990 Capability Fund and Port Hills Champion Sue Stubenvoll. J.B. thanks Sarah Trutner, Peter  
991 Borella, Maxwell Borella, David Jacobson, Sarah Bastin, Jonathan Davidson, Peter Almond,  
992 Simon Brocklehurst, David Bell, and Jarg Pettinga. Special thanks to Pip and David Barker for  
993 allowing us land access in Purau and review of the Camp Bay geotechnical property report.  
994 We also thank the Rapaki landowners and farmers for land access. The authors declare that  
995 they have no conflict of interest.

996

997 *Author Contribution*

998

999 J.B. performed the field mapping, RAMMS modeling, and was the primary contributor to the  
1000 data interpretation and manuscript authorship. M.Q. contributed to study design, data  
1001 interpretation and manuscript authorship. Z.K. performed field mapping, RAMMS modeling,  
1002 and contributed to the preparation of the manuscript. K.L. conducted the source rock  
1003 characterization at Rapaki. J.A. performed the strong ground motion analysis and contributed  
1004 to the preparation of the manuscript. L.S., H.L., and S.L. performed field mapping of rockfalls  
1005 at Purau and/or Rapaki. S.H. and D.G. performed field work and contributed to the manuscript  
1006 preparation.

1007 **References**

1008

1009 Agliardi, F. and Crosta, G. B.: High resolution three-dimensional numerical modeling of  
1010 rockfalls, *Int. J. Rock Mech. Min. Sci.*, 40, 455–471, 2003, doi:10.1016/S1365-  
1011 1609(03)00021-2.

1012

1013 Bartelt, P., Buehler, Y., Christen, M., Deubelbeiss, Y., Graf, C., and McArdell, B. W.:  
1014 RAMMS - rapid mass movements simulation: A numerical model for rockfall in research  
1015 practice, User Manual v1.5. Davos, Switzerland, 102 pp., 2013.

1016

1017 Bell, D. H. and Trangmar, B. B.: Regolith materials and erosion processes on the Port Hills,  
1018 Christchurch, New Zealand, Fifth International Symposium on Landslides, Lausanne: A. A.  
1019 Balkema, 93-105, 1987.

1020

1021 Borella J., Quigley M., and Vick, L.: Anthropocene rockfalls travel farther than prehistoric  
1022 predecessors, *Sci. Adv.*, 2, e1600969, 2016.

1023

1024 Borella, J., Quigley, M., Sohbaty, R., Almond, P., Gravley, D.M., and Murray, A.:  
1025 Chronology and processes of late Quaternary hillslope sedimentation in the eastern South  
1026 Island, New Zealand, *J. Quat. Sci.*, 31, 691-712, 2016, doi: 10.1002/jqs.2905.

1027

1028 Bouchon, M. and Barker, J. S.: Seismic response of a hill: The example of Tarzana,  
1029 California, *Seismol. Soc. Am. Bull.*, 86(1A), 66 – 72, 1996.

1030

1031 Bradley, B. A., and Cubrinovski, M.: Near-source strong ground motions observed in the 22  
1032 February 2011 Christchurch earthquake. *Seismol. Res. Lett.*, 82, 853 – 865, 2011.  
1033 <https://doi.org/10.1785/gssrl.82.6.853>

1034

1035 Bradley, B. A.: Ground motions observed in the Darfield and Christchurch earthquakes and  
1036 the importance of local site response effects, *New Zealand Journal of Geology and*  
1037 *Geophysics*, 55(3), 279 – 286, 2012. <https://doi.org/10.1080/00288306.2012.674049>

1038

1039 Bradley, B. A.: Strong ground motion characteristics observed in the 13 June 2011 Mw6.0  
1040 Christchurch, New Zealand earthquake, *Soil Dynamics and Earthquake Engineering*, 91, 23 –  
1041 38, 2016. <http://dx.doi.org/10.1016/j.soildyn.2016.09.006>

1042

1043 Burjánek, J., Gischig, V., Moore, J. R. and Fäh, D.: Ambient vibration characterization and  
1044 monitoring of a rock slope close to collapse, *Geophys. J. Int.*, 212, 297 – 310, 2018.  
1045 <https://doi.org/10.1093/gji/ggx424>

1046

1047 Carey, J. M., Misra, S., Bruce, Z. R., and Barker, P. R.: Canterbury Earthquakes 2010/11 Port  
1048 Hills Slope Stability: Laboratory Testing Factual Report, GNS Science Consultancy Report  
1049 2014/53, GNS Science, Lower Hutt, 88 pp., 2014.

1050

1051 Christensen, N. I., Wilkens, R. H. and Blair, S. C.: Seismic velocities, densities, and elastic  
1052 constants of volcanic breccia and basalts from deep sea drilling project leg 59, Initial Reports  
1053 of the Deep Sea Drilling Project, LIX, Washington, pp. 515 – 517, 1980.

1054

1055 Copons, R. and Vilaplana, J. M.: Rockfall susceptibility zoning at a large scale: From  
1056 geomorphological inventory to preliminary land use planning, *Eng. Geol.*, 102, 142–151,  
1057 2008.

1058

1059 Copons, R., Vilaplana, J. M., and Linares, R.: Rockfall travel distance analysis by using  
1060 empirical models (Sola d’Andorra la Vella, Central Pyrenees), *Nat. Hazards Earth*  
1061 *Syst. Sci.* 9, 2107–2118, 2009.

1062

1063 Dorren, L.: A review of rockfall mechanics and modelling approaches, *Prog. Phys. Geog.*,  
1064 27(1), 69–87, 2003.

1065

1066 Dorren, L., Maier, B., Putters, U. S., and Seijmonsbergen, A. C.: Combining field and  
1067 modelling techniques to assess rockfall dynamics on a protection forest hillslope in the  
1068 European Alps, *Geomorphology*, 57, 151-167, 2004, doi:10.1016/S0169-555X(03)00100-4.

1069

1070 Dussauge-Peisser, C., Helmstetter, A., Grasso, J.-R., Hantz, D., Desvarreux, P., Jeannin, M.,  
1071 and Giraud, A.: Probabilistic approach to rock fall hazard assessment: potential of historical  
1072 data analysis, *Nat. Hazards Earth Syst. Sci.*, 2, 15–26, 2002, [http://www.nat-hazards-earth-](http://www.nat-hazards-earth-syst-sci.net/2/15/2002/)  
1073 [syst-sci.net/2/15/2002/](http://www.nat-hazards-earth-syst-sci.net/2/15/2002/).

1074

1075 Eliot Sinclair and Partners Ltd., Unpublished Geotechnical Report prepared for Purau  
1076 Properties Ltd., Camp Bay Road, Purau, 18 pp., 2011.

1077

1078 Evans, S. G. and Hungr, O.: The assessment of rockfall hazard at the base of talus slopes,  
1079 *Can. Geotech. J.*, 30, 620–636, 1993.

1080

1081 Guzzetti, F., Malamud, B. D., Turcotte, D. L., and Reichenbach, P.: Power-law correlations  
1082 of landslide areas in central Italy, *Earth Planet. Sci. Lett.*, 195, 169-183, 2002.

1083

1084 Guzzetti, F., Reichenbach, P., and Wieczorek, G. F.: Rockfall hazard and risk assessment in  
1085 the Yosemite Valley, California, USA, *Nat. Hazards Earth Syst. Sci.*, 3, 491–503, 2003,  
1086 <http://www.nat-hazards-earth-syst-sci.net/3/491/2003/>.

1087

1088 Guzzetti, F., Reichenbach, P., and Ghigi, S.: Rockfall hazard and risk assessment along a  
1089 transportation corridor in the Nera Valley, Central Italy, *Environ. Manage.*, 34, 191-208,  
1090 2004, doi:10.1007/s00267-003-0021-6.

1091

1092 Hampton, S.J. and Cole, J.W.: Lyttelton Volcano, Banks Peninsula, New Zealand: Primary  
1093 volcanic landforms and eruptive centre identification, *Geomorphology*, 104, 284-298, 2009,  
1094 doi:10.1016/j.geomorph.2008.09.005.

1095

1096 Hartzell, S. H., Carver, D. L. and King, K. W.: Initial investigation of site and topographic  
1097 effects, at Robinwood Ridge, *Bull. Seismol. Soc. Am.*, 84(5), 1336 – 1349, 1994.

1098

1099 Heron, D., Lukovic, B., Massey, C., Ries, W., and McSaveney, M.: GIS modelling in support  
1100 of earthquake-induced rockfall and cliff collapse risk assessment in the Port Hills,  
1101 Christchurch. *J. Spat. Sci.* 59, 313-332, 2014, doi: 10.1080/14498596.2014.913509.

1102



1103 Kaiser, A. E., Holden, C. and Massey, C. I.: Site amplification, polarity and topographic  
1104 effects in the Port Hills during the Canterbury earthquake sequence, GNS Science  
1105 Consultancy Report 2014/121, 33 p., 2014.  
1106

1107 Keefer, D.K.: Landslides caused by earthquakes. *Geol. Soc. Am. Bull.* 95, 406-421, 1984.  
1108

1109 Kleinbrod, U., Burjánek, J., and Fäh, D.: On the seismic response of instable rock slopes  
1110 based on ambient vibration recordings, *Earth Planets Space*, 69, 126, pp. 9, 2017.  
1111 doi:10.1186/s40623-017-0712-5. <https://doi.org/10.1186/s40623-017-0712-5>  
1112

1113 Lan, H., Martin, C. D., Zhou, C., and Lim, C. H.: Rockfall hazard analysis using LiDAR and  
1114 spatial modeling, *Geomorphology*, 118, 213-223, 2010,  
1115 doi:10.1016/j.geomorph.2010.01.002.  
1116

1117 Latham, J-P., Munjiza, A., Garcia, X., Xiang, J., and Guises, R.: Three-dimensional particle  
1118 shape acquisition and use of shape library for DEM and FEM/DEM simulation, *Min. Eng.*,  
1119 21, 797-805, 2008, doi:10.1016/j.mineng.2008.05.015.  
1120

1121 Lee, S-J.: Lessons learned from source rupture to strong ground motion simulations: An  
1122 example from Taiwan, *Bull. Seismol. Soc. Am.*, 107(5), 2106 – 2116, 2017.  
1123 <https://doi.org/10.1785/0120170030>  
1124

1125 Leine, R.I., Schweizer, A., Christen, M., Glover, J., Bartelt, P., and Gerber, W.: Simulation of  
1126 rockfall trajectories with consideration of rock shape, *Multibody Syst. Dyn.*, 32, 241-271,  
1127 2013, doi:10.1007/s11044-013-9393-4.  
1128

1129 Lied, K.: Rockfall problems in Norway, in: *Rockfall dynamics and protective work*  
1130 *effectiveness*, Instituto Sperimentale Modelli e Structure (ISMES), Bergamo, Italy, 90, 51–  
1131 53, 1977.  
1132

1133 Litchfield, N. J., Van Dissen, R. J., Massey, C. I.: Pre-Christchurch earthquake sequence  
1134 rockfalls in the Port Hills, Christchurch: Wakefield Avenue Trench, GNS Science  
1135 Consultancy Report 2016/25, GNS Science, Lower Hutt, 32 pp., 2016.  
1136

1137 Mackey, B.H. and Quigley, M.C.: Strong proximal earthquakes revealed by cosmogenic <sup>3</sup>He  
1138 dating of prehistoric rockfalls, Christchurch, New Zealand. *Geology* 42, 975–978, 2014.  
1139

1140 Massey, C. I., Gerstenberger, M., McVerry, G., and Litchfield, N.: Canterbury earthquakes  
1141 2010/11 Port Hills slope stability: additional assessment of the life-safety risk from rockfalls  
1142 (boulder rolls). GNS Science Consultancy Report 2012/214, GNS Science, Lower Hutt, pp.  
1143 18, 2012a,  
1144 [http://resources.ccc.govt.nz/files/Homeliving/civildefence/chcheearthquake/gns\\_ph\\_additional](http://resources.ccc.govt.nz/files/Homeliving/civildefence/chcheearthquake/gns_ph_additional_assessmtrockfalls12687628.pdf)  
1145 [assessmtrockfalls12687628.pdf](http://resources.ccc.govt.nz/files/Homeliving/civildefence/chcheearthquake/gns_ph_additional_assessmtrockfalls12687628.pdf)  
1146

1147 Massey, C. I., McSaveney, M. J., Heron, D., and Lukovic, B.: Canterbury earthquakes  
1148 2010/11 Port Hills slope stability: pilot study for assessing life-safety risk from rockfalls  
1149 (boulder rolls). GNS Science Consultancy Report 2011/311, GNS Science, Lower Hutt, pp.  
1150 74, 2012b,  
1151 [http://resources.ccc.govt.nz/files/Homeliving/civildefence/chcheearthquake/porthills/CR2011-](http://resources.ccc.govt.nz/files/Homeliving/civildefence/chcheearthquake/porthills/CR2011-311-01AUG2013.pdf)  
1152 [311-01AUG2013.pdf](http://resources.ccc.govt.nz/files/Homeliving/civildefence/chcheearthquake/porthills/CR2011-311-01AUG2013.pdf)

1153  
1154 Massey, C. I., McSaveney, M. J., Yetton, M. D., Heron, D., Lukovic, B., and Bruce, Z. R. V.:  
1155 Canterbury earthquakes 2010/11 Port Hills slope stability: pilot study for assessing life-safety  
1156 risk from cliff collapse. GNS Science Consultancy Report 2012/57, GNS Science, Lower  
1157 Hutt, pp. 101, 2012c,  
1158 [http://resources.ccc.govt.nz/files/Homeliving/civildefence/chcheearthquake/gns\\_ph\\_pilotlifesa](http://resources.ccc.govt.nz/files/Homeliving/civildefence/chcheearthquake/gns_ph_pilotlifesa)  
1159 [fetycliffcollapse12687374web.pdf](http://resources.ccc.govt.nz/files/Homeliving/civildefence/chcheearthquake/gns_ph_pilotlifesa)  
1160  
1161 Massey, C. I., McSaveney, M. J., Lukovic, B., Heron, D., Ries, W., Moore, A., and Carey, J.:  
1162 Canterbury earthquakes 2010/11 Port Hills slope stability: life-safety risk from rockfalls  
1163 (boulder rolls). GNS Science Consultancy Report 2012/123. GNS Science, Lower Hutt, pp.  
1164 34, 2012d,  
1165 [http://resources.ccc.govt.nz/files/Homeliving/civildefence/chcheearthquake/gns\\_ph\\_lifesafetyr](http://resources.ccc.govt.nz/files/Homeliving/civildefence/chcheearthquake/gns_ph_lifesafetyr)  
1166 [ockfall12684517web-s.pdf](http://resources.ccc.govt.nz/files/Homeliving/civildefence/chcheearthquake/gns_ph_lifesafetyr).  
1167  
1168 Massey, C. I., McSaveney, M. J., and Heron, D.: Canterbury earthquakes 2010/11 Port Hills  
1169 slope stability: life-safety risk from cliff collapse in the Port Hills, GNS Science Consultancy  
1170 Report 2012/124, GNS Science, Lower Hutt, pp 35., 2012e,  
1171 [http://resources.ccc.govt.nz/files/Homeliving/civildefence/chcheearthquake/gns\\_ph\\_lifesafetyc](http://resources.ccc.govt.nz/files/Homeliving/civildefence/chcheearthquake/gns_ph_lifesafetyc)  
1172 [liffcollapse12684515web-s.pdf](http://resources.ccc.govt.nz/files/Homeliving/civildefence/chcheearthquake/gns_ph_lifesafetyc)  
1173  
1174 Massey, C. I., Yetton, M. J., Carey, J., Lukovic, B., Litchfield, N., Ries, W., and McVerry,  
1175 G.: Canterbury earthquakes 2010/11 Port Hills slope stability: stage 1 report on the findings  
1176 from investigations into areas of significant ground damage (mass movements), GNS Science  
1177 Consultancy Report 2013/317, GNS Science, Lower Hutt, pp. 37, 2013,  
1178 <http://resources.ccc.govt.nz/files/Homeliving/civildefence/chcheearthquake/porthills/CR2012->  
1179 [317Stage1.pdf](http://resources.ccc.govt.nz/files/Homeliving/civildefence/chcheearthquake/porthills/CR2012-)  
1180  
1181 Massey, C. I., McSaveney, M. J., Taig, T., Richards, L., Litchfield, N. J., Rhoades, D. A.,  
1182 McVerry, G. H., Lukovic, B., Heron, D. W., Ries, W., and Van Dissen, R. J.: Determining  
1183 rockfall risk in Christchurch using rockfalls triggered by the 2010-2011 Canterbury  
1184 earthquake sequence, *Earthquake Spectra*, 30, 155-181, 2014, DOI:  
1185 10.1193/021413EQS026M.  
1186  
1187 Massey, C., Della Pasqua, F., Holden, C., Kaiser, A., Richards, L., Wartman, J., McSaveney,  
1188 M. J., Archibald, G., Yetton, M., and Janku, L.: Rock slope response to strong earthquake  
1189 shaking. *Landslides* 14, 249-268, 2017, doi:10.1007/s10346-016-0684-8.  
1190  
1191 Muktar, J-A. S.: Engineering geological and geotechnical characterization of selected Port  
1192 Hills lavas, Master's thesis, Department of Geological Sciences, University of Canterbury,  
1193 New Zealand, pp. 172, 2014.  
1194  
1195 Porter, S. C. and Orombelli, G.: Alpine rockfall hazards: Recognition and dating of rockfall  
1196 deposits in the western Italian Alps lead to an understanding of the potential hazards of giant  
1197 rockfalls in mountainous regions, *Am. Sci.*, 69, 67-75, 1981,  
1198 <https://www.jstor.org/stable/27850249>.  
1199  
1200 Quigley M. C., Hughes, M. W., Bradley, B. A., van Ballegooy, S., Reid, C., Morgenroth, J.,  
1201 Horton, T., Duffy, B., and Pettinga, J. R.: The 2010-2011 Canterbury Earthquake Sequence:  
1202 Environmental effects, seismic triggering thresholds and geological legacy, *Tectonophysics*,

1203 672-673, 228-274, 2016.  
1204  
1205 Sewell, R.J.: Late Miocene volcanic stratigraphy of central Banks Peninsula, Canterbury,  
1206 New Zealand, *New Zeal. J. Geol. Geop.*, 31, 41-64, 1988,  
1207 doi:10.1080/00288306.1988.10417809.  
1208  
1209 Sohbaty, R., Borella, J., Murray, A., Quigley, M., Buylaert, J.: Optical dating of loessic  
1210 hillslope sediments constrains timing of prehistoric rockfalls, Christchurch, New Zealand.  
1211 *Journal of Quaternary Science*, 31, 678-690, 2016, doi: 10.1002/jqs.2895.  
1212  
1213 Spetzler, J. and Snieder, R.: The Fresnel volume and transmitted waves, *Geophysics*, 69(3),  
1214 653 – 663, 2004. <https://doi.org/10.1190/1.1759451>  
1215  
1216 Stock, G. M., Luco, N., Collins, B. D., Harp, E. L., Reichenbach, P., Frankel, K. L.:  
1217 Quantitative rock-fall hazard and risk assessment for Yosemite Valley, Yosemite National  
1218 Park, California: U.S. Geological Survey Scientific Investigations Report 2014-5129, 52 p.,  
1219 2014.  
1220  
1221 Takemura, S., Furumura, T. and Maeda, T.: Scattering of high-frequency seismic waves  
1222 caused by irregular surface topography and small-scale velocity inhomogeneity, *Geophys. J.*  
1223 *Inter.*, 201(1), 459–474, 2015. <https://doi.org/10.1093/gji/ggv038>  
1224  
1225 Townsend, D. B., Rosser, B.: Canterbury earthquakes 2010/2011 Port Hills slope stability:  
1226 Geomorphology mapping for rockfall risk assessment, GNS Science Consultancy Report  
1227 2012/15, GNS Science, Lower Hutt, pp. 21, 2012.  
1228  
1229 Van Houtte, C., Ktenidou, O.-J., Larkin, T., and Kaiser, A.: Reference stations for  
1230 Christchurch, *Bulletin of the New Zealand Society for Earthquake Engineering*, 45(4), 184 –  
1231 195, 2012.  
1232  
1233 Varnes, D. J.: Slope movement types and processes, in: *Landslides: analysis and control*,  
1234 edited by: Schuster, R. L. and Krizek, R. L., Transportation Research Board, National  
1235 Research Council, Washington, special report 176, 11–33, 1978.  
1236  
1237 Vick, L.M., Zimmer, V., White, C., Massey, C., and Davies, T.: Significance of substrate soil  
1238 moisture content for rockfall hazard assessment. *Nat. Hazards Earth Syst. Sci.* 19, 1105-1117,  
1239 2019.  
1240  
1241 Vick, L.M.: Evaluation of field data and 3D modelling for rockfall hazard assessment, Ph.D.  
1242 thesis, Department of Geological Sciences, University of Canterbury, New Zealand, pp. 173,  
1243 2015.  
1244  
1245 Wieczorek, G. F.: Catastrophic rockfalls and rockslides in the Sierra Nevada, USA. *Geol.*  
1246 *Soc. Am. Rev Eng. Geol.*, 15, 1-26, 2002.  
1247  
1248 Wieczorek, G. F., Stock, G. M., Reichenbach, P., Snyder, J. B., Borchers, J.W., and Godt,  
1249 J.W.: Investigation and hazard assessment of the 2003 and 2007 Staircase Falls rock falls,  
1250 Yosemite National Park, California, USA, *Nat. Hazards Earth Syst. Sci.*, 8, 421–432, 2008,  
1251 <http://www.nat-hazards-earth-syst-sci.net/8/421/2008/>.

	<i>Rapaki Pre-CES</i> (n=409)	<i>Rapaki CES</i> (n=48)	<i>Difference</i>	<i>Difference</i>	<i>Purau Pre-CES</i> (n=684)	<i>Purau CES</i> (n=136)	<i>Difference</i>	<i>Difference</i>
	(m <sup>3</sup> )	(m <sup>3</sup> )	(m <sup>3</sup> )	(%)	(m <sup>3</sup> )	(m <sup>3</sup> )	(m <sup>3</sup> )	(%)
25 <sup>th</sup> (Q1)	1.60	1.36	0.24	17.65	1.42	1.34	0.08	5.97
Median	2.94	2.21	0.73	33.03	2.20	2.01	0.19	9.45
75 <sup>th</sup> (Q3)	6.59	4.83	1.76	36.44	5.08	4.46	0.62	13.90
95 <sup>th</sup>	20.54	19.76	0.78	3.95	27.06	17.66	9.4	53.23
Maximum	200.56	28.35	172.21	607.44	616.00	79.97	536.03	670.29
Mean	6.81	4.84	1.97	40.70	8.10	5.32	2.78	52.26

1252  
1253  
1254  
1255

**Table 1.** Volumetric comparison of pre-CES and CES rockfall boulders (for volume  $\geq 1.0$  m<sup>3</sup>) at Rapaki and Purau study sites.

	<i>Rapaki</i>				<i>Purau</i>			
	Pre-CES	CES	Pre-CES	CES	Pre-CES	CES	Pre-CES	CES
	VB (n=391) (m <sup>3</sup> )	VB (n=45) (m <sup>3</sup> )	CL (n=18) (m <sup>3</sup> )	CL (n=3) (m <sup>3</sup> )	VB (n=436) (m <sup>3</sup> )	VB (n=127) (m <sup>3</sup> )	CL (n=248) (m <sup>3</sup> )	CL (n=9) (m <sup>3</sup> )
25 <sup>th</sup> (Q1)	1.68	1.39	1.22	1.03	1.70	1.36	1.20	1.13
Median	3.1	2.21	1.38	1.06	3.21	2.04	1.56	1.68
75 <sup>th</sup> (Q3)	6.78	5.7	1.54	1.67	7.65	4.87	2.30	2.14
95 <sup>th</sup>	21.28	20.576	3.92	2.16	40.91	17.78	5.26	2.48
Maximum	200.56	28.35	9.99	2.28	616.00	79.97	26.21	2.64
Mean	7.03	5.06	1.96	1.45	11.43	5.58	2.24	1.67
Total volume	2749.07	227.80	35.29	4.34	4938.76	708.34	555.63	15.00
% of total volume	99	98	1	2	89	98	11	2
% of mapped boulders	96	94	4	6	64	93	36	7

1256  
1257  
1258  
1259  
1260  
1261  
1262

**Table 2.** Comparison of boulder size statistics for Rapaki and Purau VB and CL pre-CES and CES rockfall boulders (volume  $\geq 1.0$  m<sup>3</sup>).

	<i># of pre-CES rockfalls :</i> <i># of CES rockfalls</i>	<i>pre-CES : CES</i>	<i>pre-CES : CES</i>	<i>volume of pre-CES rockfalls:</i> <i>volume of CES rockfalls</i>	<i>pre-CES : CES</i>	<i>pre-CES : CES</i>
	(n)	ratio	% : %	(m <sup>3</sup> )	ratio	% : %
Total (Rapaki + Purau)	1093 : 184	5.94	86 : 14	8323.76 : 955.48	8.71	90 : 10
Rapaki Total	409 : 48	8.52	89 : 11	2784.37 : 232.14	11.99	92 : 8
Rapaki VB	391 : 45	8.69	90 : 10	2749.07 : 227.80	12.07	92 : 8
Rapaki CL	18 : 3	6.00	86 : 14	35.29 : 4.34	8.14	89 : 11
Purau Total	684 : 136	5.03	83 : 17	5539.39 : 723.35	7.66	88 : 12
Purau VB	436 : 127	3.43	77 : 23	4983.76 : 708.34	7.04	88 : 12
Purau CL	248 : 9	27.56	96 : 4	555.63 : 15.00	37.04	97 : 3

1263  
1264  
1265  
1266

**Table 3A.** Comparison of frequency (n) and volume (m<sup>3</sup>) ratios for pre-CES and CES rockfall boulders at the Rapaki and Purau study sites.

	<i># of VB boulders :</i> <i># of CL boulders</i>	<i>VB : CL</i>	<i>VB : CL</i>	<i>Volume of VB boulders :</i> <i>volume of CL boulders</i>	<i>VB:CL</i>	<i>VB:CL</i>
	n : n	ratio	% : %	m <sup>3</sup> : m <sup>3</sup>	ratio	% : %
Total (Rap + Purau)	999 : 278	3.59	78 : 22	8668.97 : 610.26	14.21	93 : 7
Rapaki Total (pre-CES + CES)	436 : 21	20.76	95 : 5	2976.87 : 39.63	75.11	99 : 1
Rapaki pre-CES	391 : 18	21.72	96 : 4	2749.07 : 35.29	77.9	99 : 1
Rapaki CES	45 : 3	15	94 : 6	227.80 : 4.34	52.49	98 : 2
Purau Total (pre-CES + CES)	563 : 257	2.19	69 : 31	5692.1 : 570.63	9.98	91 : 9
Purau pre-CES	436 : 248	1.76	64 : 36	4983.76 : 555.63	8.97	90 : 10
Purau CES	127 : 9	14	93 : 7	708.34 : 15.00	47.22	98 : 2
Purau D1 pre-CES	17 : 0	N/A	100 : 0	137.27 : 0	N/A	100 : 0
Purau D1 CES	30 : 0	N/A	100 : 0	125.86 : 0	N/A	100 : 0
Purau D2 pre-CES	36 : 3	12	92 : 8	230.8 : 3.9	59.18	98 : 2
Purau D2 CES	1 : 1	1	50 : 50	14.78 : 1.08	13.69	93 : 7
Purau D3 pre-CES	54 : 43	1.26	56 : 44	203.79 : 142.62	1.43	59 : 41
Purau D3 CES	38 : 3	12.67	93 : 7	242.63 : 5.91	41.05	98 : 2
Purau D4 pre-CES	8 : 1	8	89 : 11	188.42 : 1.24	151.95	99 : 1
Purau D4 CES	36 : 0	N/A	100 : 0	267.76 : 0	N/A	100 : 0

1267  
1268

**Table 3B.** Comparison of VB/CL frequency (n) and volume (m<sup>3</sup>) ratios for pre-CES and CES rockfall boulders at the Rapaki and Purau study sites.

<b>Runout Distance (MLR)</b>	<i>Average</i>	<i>Maximum</i>
	(m)	(m)
<b>Rapaki</b>		
Pre-CES	184.30	567.51
CES	276.23	702.47
<i>Pre-CES VB</i>	<i>184.65</i>	<i>567.51</i>
<i>Pre-CES CL</i>	<i>176.57</i>	<i>346.73</i>
<i>CES VB</i>	<i>276.91</i>	<i>702.47</i>
<i>CES CL</i>	<i>266.13</i>	<i>432.14</i>
<b>Purau</b>		
PD1 Pre-CES	29.86	96.96
PD1 CES	119.63	348.4
PD2 Pre-CES	84.01	279.75
PD2 CES	14.11	15.91
PD3 Pre-CES	239.62	462.8
PD3 CES	237.24	413.35
PD4 Pre-CES	109.11	208.85
PD4 CES	181.75	304.56
<i>PD1 Pre-CES VB</i>	<i>29.86</i>	<i>96.96</i>
<i>PD1 CES VB</i>	<i>119.63</i>	<i>348.4</i>
<i>PD1 Pre-CES CL</i>	<i>N/A</i>	<i>N/A</i>
<i>PD1 CES CL</i>	<i>N/A</i>	<i>N/A</i>
<i>PD2 Pre-CES VB</i>	<i>88.73</i>	<i>279.75</i>
<i>PD2 CES VB</i>	<i>12.3</i>	<i>12.3</i>
<i>PD2 Pre-CES CL</i>	<i>27.39</i>	<i>33.38</i>
<i>PD2 CES CL</i>	<i>15.91</i>	<i>15.91</i>
<i>PD3 Pre-CES VB</i>	<i>248.96</i>	<i>434.85</i>
<i>PD3 CES VB</i>	<i>243.21</i>	<i>413.35</i>
<i>PD3 Pre-CES CL</i>	<i>227.89</i>	<i>462.8</i>
<i>PD3 CES CL</i>	<i>161.68</i>	<i>178.53</i>
<i>PD4 Pre-CES VB</i>	<i>106.99</i>	<i>208.85</i>
<i>PD4 CES VB</i>	<i>181.75</i>	<i>304.56</i>
<i>PD4 Pre-CES CL</i>	<i>126.06</i>	<i>126.06</i>
<i>PD4 CES CL</i>	<i>N/A</i>	<i>N/A</i>

MLR = Map Length Runout  
PD1 = Purau Domain 1

**Table 4.** Average and maximum runout distances for pre-CES and CES rockfall boulders (for volume  $\geq 1.0 \text{ m}^3$ ) at Rapaki and Purau study sites.

## Figure Captions

**Fig. 1. (A)** Google Earth image showing Rapaki and Purau study sites. CES rockfall locations as mapped by GNS Science and the author (at Rapaki and Purau) are shown (red). Epicenter locations for 22 February, 13 June, and 16 April 2011 events are displayed [Modified from Massey et al. (2014)]. Inset map of South Island (New Zealand) shows Banks Peninsula and approximate location for study site (yellow star). **(B)** Anthropogenic deforestation of Banks Peninsula. Removal of native forest occurred rapidly in Banks Peninsula (BP) with arrival of Polynesians (c. AD 1280) then Europeans (c. AD 1830). Before Polynesian (Maori) arrival, extensive native forest was present throughout BP. Prior to European settlement, minor to moderate removal of indigenous forest by Maori occurred, with burning being the primary tool for clearance (yellow). By 1920 Europeans had removed >98% of BP native forest (red). Minor re-establishment of old-growth native forest has occurred (green) but slopes in the Port Hills and greater BP (including Rapaki and Purau) remain largely unvegetated.

**Fig. 2. (A)** Mapped pre-CES volcanic breccia (VB) and coherent lava (CL) boulders at Rapaki. The largest boulders with the furthest runout distances are comprised exclusively of volcanic breccia. Ratio of pre-CES VB to CL boulders is ~22:1. **(B)** Mapped CES VB and CL boulders at Rapaki study site. Note the low number of CL rockfall boulders detached during the CES at Rapaki. Ratio of CES VB to CL boulders is 15:1. [a = volcanic source rock; b = dominated by volcanic boulder colluvium and volcanic loess colluvium; c = loess-colluvium underlain by in-situ loess and volcanic rock; d = alluvial sediments overlying loess and bedrock]

**Fig. 3. (A)** Mapped pre-CES and CES rockfalls with volume  $\geq 1.0 \text{ m}^3$  at Purau study site. Ratio of pre-CES to CES boulders is ~5:1. A= volcanic source rock; B=dominated by volcanic boulder colluvium and volcanic loess colluvium; C=loess-colluvium underlain by in-situ loess and volcanic rock; D=alluvial sediments overlying loess and bedrock. **(B)** Mapped pre-CES VB and CL boulders at Purau. Ratio of pre-CES VB to CL boulders is ~2:1. **(C)** Mapped CES VB and CL boulders at Purau study site. Note the low number of CL rockfall boulders detached during the CES at Purau. Ratio of CES VB to CL boulders is ~14:1. PD1-PD4 represent Purau rockfall domains.

**Fig. 4.** Pre-CES and CES VB boulders at Rapaki and Purau study sites. **(A)** Pre-CES boulder in footslope position with smaller CES boulder at right bottom. **(B)** Exploratory trenching exposes the colluvial sediment wedge at the boulder backside depicted in Fig. 7B. **(C)** Pre-CES boulder at Purau study site. Erosion of the surrounding hillslope sediments has exposed the boulder base and underlying loessic sediment. **(D)** Advanced surface roughness and abundant lichen growth on pre-CES boulder surface. **(E)** Large CES boulder (~28 m<sup>3</sup>) detached from Mount Rapaki and emplaced in the Rapaki village during the 22 February 2011 earthquake (photo courtesy of D.J.A. Barrell, GNS Science). **(F)** CES boulder showing 2011 detachment surface [1] and adjacent non-detached surface [2] with higher degree of rough. **(G-K)** Representative CL boulders at Rapaki and Purau sites exhibit typical elongate and flat morphologies.

**Fig. 5. (A)** Volcanic source rock at Rapaki study site. Sixty (60) individual detachment zones were created during the CES (yellow) and represent ~9% of the total source rock area. The source rock is comprised of ~86% VB and ~14% CL. ~69% and ~31% of the detachments occurred within the VB and CL lithologies, respectively. **(B)** Photo showing

several irregularly shaped CES detachment zones near the top of Mt. Rapaki. **(C)** Photo showing freshly exposed VB and CL layering within the Rapaki source rock. **(D)** Portion of volcanic source rock at Purau showing VB and CL layering. A single CES detachment site is shown at the top of the source rock. Seven (7) individual CES detachment sites were identified at the Purau study site. **(E)** CL and VB layers at the Purau study site. Note the thickness of the CL layer (~5-7 meters) and lack of any CES detachment sites despite the high degree of fracturing and overhanging condition. **(F)** VB and CL layering in Sumner (Christchurch) cliff exposure adjacent to Main Road. Extensive cliff collapse during the CES has revealed multiple lava flows and the distinctive textural differences between the VB and CL lithologies. Note the high density of vertical to subvertical fractures within the CL layers. **(G)** Exposed lava layers adjacent to Main Road in Redcliffs (Christchurch). Note the single-family living residence at top of photo.

**Fig. 6.** Relative locations of stations LPCC, D13C, D15C, and GODS (yellow squares). Also shown are epicentres of 2011-02-21 Mw 6.2 and 2011-06-13 Mw 6 earthquakes (yellow stars) along with Rapaki and Purau sites.

**Fig. 7.** Each panel shows seismic data from LPCC (A and B), D13C (C), D15C (D), and GODS (E) stations. Panels A and B compare ground motion, respectively, for 2011-02-21 Mw 6.2 and 2011-06-13 Mw 6 earthquakes at LPCC station. The left column shows east and north components of the velocity seismogram (blue line) and their respective envelopes (red dashed-line). The particle velocity hodogram (middle column, green line) was determined for a time window  $\pm 5$  s (shaded region in the left column) around the peak (red circle) of the east component envelope. The strike of the rock face (black short line segments) and the direction of the free face (red arrows) for sites PD1, PD2, PD3, PD4, and RAP are also illustrated. The particle motion hodogram (grey line) is presented in the right column, where green, yellow, and red segments represent, respectively, time points at which east component, north component, or both components exceed an acceleration of 0.3g. Note that scale of figure axes varies by station particularly for ground motion.

**Fig. 8.** **(A)** Rockfall size distribution as a proportion of boulders less than a given size plotted in log-space for CES and pre-CES rockfalls at Rapaki. **(B)** Rockfall frequency/size distribution for CES and pre-CES rockfalls at Rapaki. **(C)** Rockfall size distribution as a proportion of boulders less than a given size plotted in log-space for CES and pre-CES rockfalls at Purau. **(D)** Rockfall frequency/size distribution for CES and pre-CES rockfalls at Purau. **(E)** Comparison of boulder size distributions for CES and pre-CES VB and CL rockfalls at Rapaki study site. **(F)** Comparison of boulder size distributions for CES and pre-CES VB and CL rockfalls at Purau.

**Fig. 9.** **(A)** Frequency ratio versus volume ratio for pre-CES and CES rockfall boulders. **(B)** Frequency-runout distributions for Rapaki pre-CES and CES boulders. Both power law (without extrapolated data) and exponential fits (all data) are shown for the prehistoric boulder data set. A poor exponential fit is shown for CES rockfalls. **(C)** Plot of travel distance on talus slope (Lt) versus height on talus slope (Ht) with fitted polynomial regression lines for pre-CES and CES rockfalls at Rapaki. **(D)** Plot of Lt versus Ht with fitted linear, log, and polynomial regression lines for pre-CES and CES rockfalls at Purau. Four (4) separated domains (here D1-D4) are defined at Purau to evaluate the shadow angle method. **(E)** Plot of rockfall size ( $m^3$ ) versus tangent of the shadow angle (Ht/Lt) for Rapaki rockfalls. No tendency of the data is evident. **(F)** Plot of rockfall size ( $m^3$ ) versus tangent of the shadow



angle (Ht/Lt) for Purau rockfalls. The tendency for the domain data sets is poor. Values of correlation coefficients are below 0.3.

**Fig. 10.** (A) RAMMS\_1 shows deposited rocks (Q 95%) for simulated CES boulders. Mapped CES boulders (red circles; n=136) are shown for comparison. Boulder densities of 2500 kg/m<sup>3</sup> and 3000 kg/m<sup>3</sup> are used for VB and CL boulders, respectively. (B) Final resting locations (Q 95%) for RAMMS\_2 rockfalls. RAMMS\_2 assumes prehistoric rockfall conditions (i.e. forested hillslope). Mapped prehistoric rockfalls are depicted (yellow circles) for comparison. An increase in forest density to 10,000 kg/s generates the best fit with maximum runout distance (see white dashed line) for mapped prehistoric boulders. (C) Final resting locations for RAMMS\_3 boulders (Q 95%). RAMMS\_3 assumes modern hillslope conditions (i.e. deforested hillslope) and simulates the future potential rockfall hazard at Purau. The modelling indicates that the distribution of future rockfalls could be widespread and more impactful to existing and proposed development than experienced during the CES.

**Fig. 11.** RAMMS simulated rockfall boulders showing differences in spatial distribution between VB (mostly equant shaped) and CL (predominantly elongate and flat shaped) boulder morphologies at Purau. All simulated boulders assume a volume of 1.0 m<sup>3</sup>. (A) Spatial distribution of simulated VB boulders at Purau CES-7 location. Note the high relative percentage of simulated boulders deposited at the base of the hillslope (~500-600 meters from source rock). (B) Spatial distribution of simulated CL boulders at CES-7 location. Note the higher relative percentage of rockfall boulders deposited near the source rock (within ~100 meters from source rock). The simulation highlights the strong influence of boulder shape on runout distance.

**Fig. 12.** CES and pre-CES rockfall boulders within drainage valleys at Rapaki (A, C) and Purau (B, D, E, F) study locations. Drainage valleys contain a high amount of pre-CES rockfall boulders, which impacts the trajectory/path of CES rockfalls and stops or reduces runout distance.

**Fig. 13.** Velocity spectra for the 2011-06-13 Mw 6 earthquake recorded at station D13C. No path corrections are applied.

## Appendix 1 - Captions

**Fig. A1.** The total number of boulders with volume  $\geq 0.1 \text{ m}^3$  were taken at runout distances of 1-10 m (yellow polygon 1), 30-40 m (yellow polygon 2), 60-70 m (yellow polygon 3), and 100-110 m (yellow polygon 4) from the volcanic source rock to estimate the total number of boulders in areas near the source cliff where conditions were unsafe for continuous mapping. The number of boulders in areas 'b' and 'c' were reduced by factors of 2 and 3, respectively, based upon field observations. The total number of rockfalls boulders for the area (yellow dashed line) was normalized to boulder size of  $1.0 \text{ m}^3$  using a power law frequency-size distribution (as determined at the Rapaki study location).

**Fig. A2.** Conceptual diagram of hillslope illustrating the source rock cliff and the talus slope. The reach angle (A) and shadow angle (B) are shown. Sketch modified from Hungr (1993), Wieczorek et al. (2008) and Copons et al. (2009).

**Fig. A3.** Final resting locations for RAMMS\_2 rockfalls assuming uniform forest density increase of 10,000 kg/s.

## Appendix 2 - Captions

**Table A1.** Friction parameters chosen for each terrain type in RAMMS.

**Fig. A1.** Polygon shapefiles for runout terrain types.

**Fig. A2.** Polyline shapefiles for RAMMS\_1 rockfall source areas.

**Fig. A3.** Polyline shapefiles for RAMMS\_2 and RAMMS\_3 rockfall source areas.

**Fig. A4** Polygon shapefiles for forest density.

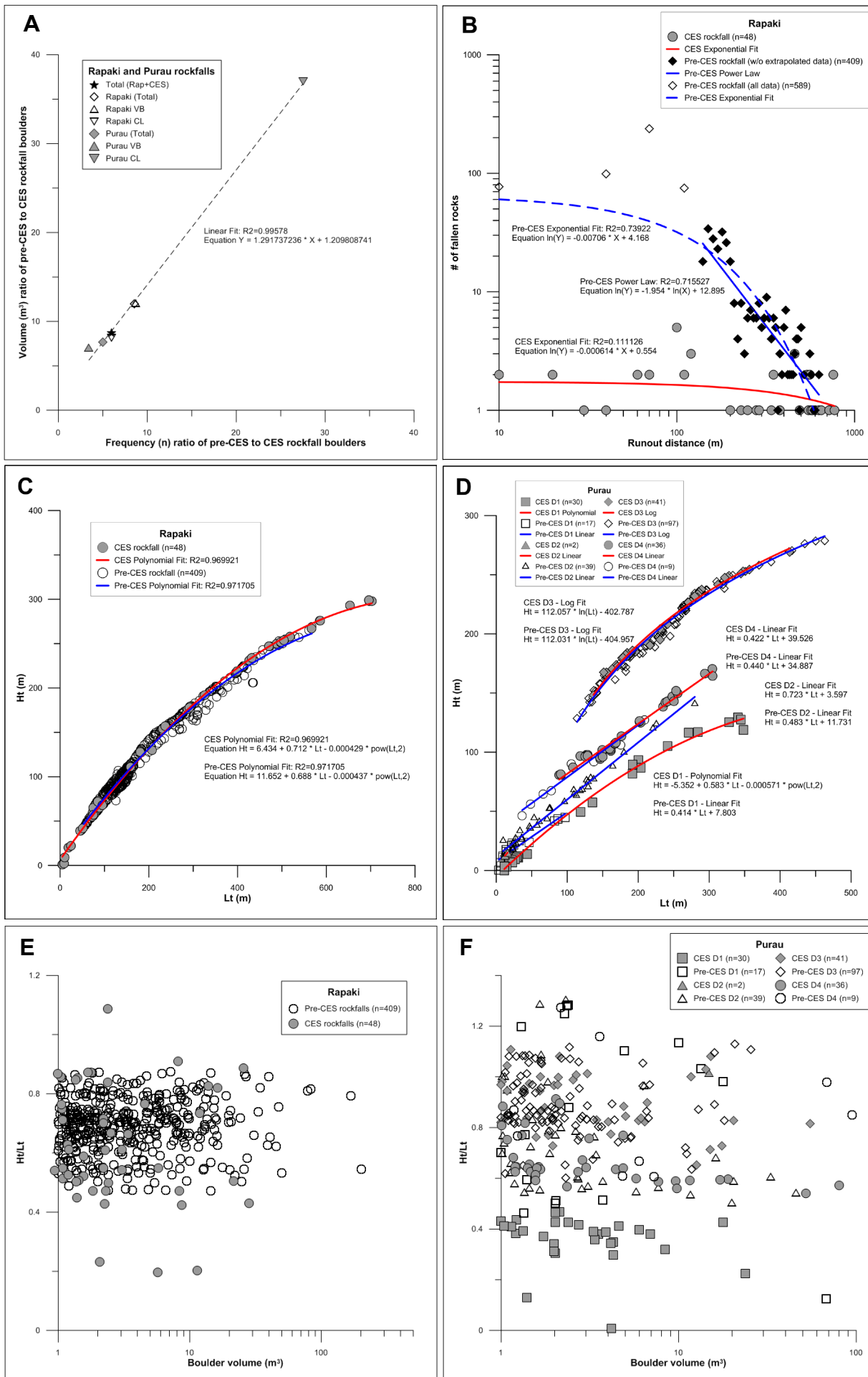


Figure 9